Designing autonomous Maxwell's demon via stochastic resetting

Ruicheng Bao,[*] Zhiyu Cao,[*] Jiming Zheng,[*] and Zhonghuai Hou[†]
Department of Chemical Physics & Hefei National Laboratory for Physical Sciences at Microscales, iChEM, University of Science and Technology of China, Hefei, Anhui 230026, China

(Received 26 September 2022; accepted 9 October 2023; published 20 October 2023)

Autonomous Maxwell's demon is a new type of information engine proposed by Mandal and Jarzynski [Proc. Natl. Acad. Sci. USA **109**, 11641 (2012)], which can produce work by exploiting an information tape. Here, we show how stochastic resetting can notably enhance the performance of autonomous Maxwell's demons in two ways: the speed of reaching their functional states and the range of their effective work regions. We propose some design principles for this system using stochastic resetting. Firstly, one can drive any autonomous demon system to its functional periodic steady state at a fastest pace from any initial distribution through resetting the demon for a predetermined critical time and then stopping the reset. Secondly, we can make the system achieve a new functional state with a larger effective working region by keeping the reset on. We also discover a dual-function region in a new phase diagram of the demon with resetting, where the demon can remarkably produce work and erase information on the tape at the same time, apparently breaking the second law of thermodynamics. We resolve this paradox by deriving a modified Clausius inequality that includes the cost of resetting.

DOI: 10.1103/PhysRevResearch.5.043066

I. INTRODUCTION

In 1867 [1], James C. Maxwell conceived the thought experiment of Maxwell's demon, a hypothetical creature that can use information to apparently violate the second law of thermodynamics. In 1961, Rolf Landauer and Charles Bennett showed that Maxwell's demon does not actually violate the second law of thermodynamics [2,3]. They demonstrated that the demon must expend energy to store the information gained from measurements, which upholds the validity of the second law of thermodynamics. Maxwell's demon thought experiment has led to a series of interdisciplinary studies focusing on the interplay between information theory and thermodynamics. Recent years have witnessed great progress in this field known as information thermodynamics, including fruitful experimental [4] and theoretical studies [5].

Over the past 150 years, Maxwell's-demon-like models have undergone extensive theoretical scrutiny [5–8]. These models can be broadly classified into two categories: measurement-feedback-controlled demons and autonomous demons. On the one hand, T. Sagawa and M. Ueda have developed the theoretical framework for the first class of measurement-feedback demons [9]. On the other hand, Mandal and Jarzynski have constructed two analytically solvable autonomous demon models [8,10], each consisting of a memory tape and a demon. These memory-tape autonomous demons can realize processes that apparently defy the second law of thermodynamics by exploiting information. Subsequent research has delved into these two types of Maxwell's demon models, resulting in a rich body of papers [11–19]. Additionally, both of these demon models have been further extended to quantum systems [20–22].

Stochastic resetting, a rather common driving mechanism that randomly halts and restarts a dynamical process, has recently captured significant attention in the field of statistical physics [23–32]. It has been revealed that stochastic resetting can, counterintuitively, accelerate dynamical processes on average. For instance, Evans and Majumdar [23] were the first to theoretically investigate stochastic resetting, demonstrating that the mean time for a freely diffusing Brownian particle to reach a fixed target becomes finite with constant-rate Poisson resetting, whereas it diverges without resetting. Subsequently, the benefits of resetting have been observed in various stochastic processes in real world, including animal foraging, RNA polymerase backtrack recovery [33], and relaxation processes [34]. Furthermore, the effect of stochastic resetting on thermodynamics is also of interest [35–40]. For more discussions on stochastic resetting, refer to two recent reviews [41,42]. Generally, this stochastic resetting mechanism could be used to optimize controlling protocols in small systems.

Autonomous demons possess two critical features that are central to evaluating their performance. The first feature is the relaxation timescale required for the demon to attain its functional periodic steady state [43]. It would be more experimentally accessible to initially prepare the demon in an equilibrium state, typically distinct from the periodic steady state. This incurs a time cost as the demon transitions into

[*]These authors contributed equally to this work.
[†]hzhlj@ustc.edu.cn

its working state, where it begins converting information resources into work. The phase before working state is often referred to as the warming-up phase in the literature [44]. In most cases, minimizing the time cost associated with the demon's initial deviation from the functional state is desirable, leading to a shorter warming-up phase. The demons operate effectively in two key regions: one where they can produce positive work by harnessing information resources (the information engine region) and another where they function as erasers, replenishing information resources (the information eraser region, characterized by the decrease in the information entropy of the memory tape on average). The second crucial feature is the scope of these two functional regions. One would desire to extend these two regions of the demon to enhance its performance.

In the current study, we employ a discrete-time stochastic resetting mechanism to establish design principles for the autonomous Maxwell's demons. The mechanism can enhance the demon's performance in two critical aspects: the time cost and the effective working regions. To achieve control over these key features of the autonomous demon, we introduce two distinct resetting strategies, one aimed at reducing time cost and the other at expanding the useful working regions. The first strategy involves resetting the demon to a predefined state with a constant probability at discrete-time intervals (typically at the end of each cycle) for a fixed duration, denoted as t_c. Subsequently, we stop the reset and allow the demon to evolve according to its original dynamics. Strikingly, this approach can drive the demon to reach its functional periodic steady state at the fastest pace, regardless of its initial distribution. This acceleration strategy draws inspiration from the so-called "strong" Mpemba effect, which recently aroused widespread attention [45–50]. The second strategy entails ceaseless resetting of the demon to a specified state, leading the demon system to ultimately reach a new periodic steady state, the characteristics of which differ from the original autonomous demon. In the phase diagram of this modified autonomous demon with resetting, the information engine region is extended while the information eraser region remains largely unchanged. Remarkably, an overlapping region, which we term the "dual-function region," emerges in the new phase diagram. In this region, the second law of thermodynamics is apparently violated. To restore the second law, we derive aClausius inequality that incorporates an additional term resulting from the stochastic resetting effect, which restores the second law of thermodynamics in the presence of resetting.

This article is organized as follows. In Sec. II, we present the methods employed to analyze autonomous Maxwell's demon models introduced by Mandal and Jarzynski. Moreover, the formalism of discrete-time stochastic resetting is introduced. Moving on to Sec. III, we delve into our approach for inducing significantly faster relaxations of the autonomous demon towards functional periodic steady states through the utilization of stochastic resetting strategies. Section IV unveils phase diagrams for an autonomous demon operating with incessant resetting, where we observe an expansion of the anomalous work region and the emergence of a fascinating "dual-function" region. In Sec. V, we make some discussions and conclude the paper.

II. MODEL AND FRAMEWORK

In this section, we first briefly review the autonomous demon model. Subsequently, we introduce the discrete-time stochastic resetting mechanism, an extension intended for incorporation into the original autonomous demon framework.

Preliminary: The autonomous demon. An autonomous Maxwell's demon consists of a demon with k states and an infinitely long memory tape (a stream of bits) encoding information with bit 0 and 1. In our setup, the k-state demon is initially in equilibrium with a thermal reservoir at temperature $T_{\rm in}$, then it will be coupled to a memory tape to constitute a $2k$ states combined system. This memory tape plays the roles of measurement and feedback as in the conventional Maxwell's demon system. The tape moves through the demon frictionlessly at a constant speed to a given direction, with the bit sequence on it written in advance (e.g., 011100...). The bit sequence is described by a probability distribution $\boldsymbol{p}^B_{\rm in} = (p_0, p_1)^{\rm T}$, where p_1 and p_0 are the probabilities of the incoming bit to be in states 1 and 0. For later use, we define $\delta \equiv p_0 - p_1$ as the proportional excess of 0's among all incoming bits in the tape. The demon interacts with the incoming bits one by one as they pass by, i.e., it only interacts with the nearest bit for a fixed time τ, after that the current bit leaves and a new bit comes in. During each interaction interval, the demon undergoes intrinsic transitions between some pair of states. The bit can also transition between state 0 and 1, and the demon's transition is coupled to the bit's transition. These type of cooperative transitions cannot occur in the absence of either the demon or the bit. These cooperative transitions can lead to anomalous work production. The demon's disordered transitions (which are similar to fluctuations) can be rectified by the incoming bits, which is the key idea of the autonomous demon. If the outgoing bit stream becomes more disordered than the incoming bit stream (the information entropy of the bit increase), then the transition of the demon is rectified on average to a given direction. The transition to this direction can produce work at the cost of information resources, while the transition to the opposite direction produces no work. The direction of transition that produces positive work depends on the setup of the combined system. In this paper, we set the transition of bit from 0 to 1 as the desired event. This can rectify the demon's transitions to a given direction, producing positive output work. Therefore, 0 is the information resource that can be consumed to drive the system to the desired direction. Then, a quantity $\delta = p_0 - p_1$ can be introduced to quantify the information resource. The larger the δ is, the more information resource is contained in the tape. When $\delta = 1$, the tape contains the maximum amount of information resource, since all of the bits are 0.

Before proceeding, we list some notations for later use. Importantly, $t_N := N\tau$ is the beginning time of the $(N+1)$th interaction interval, with τ being the interaction time of each interval. $\boldsymbol{p}^D(t)$ is a column vector with k entries, which describes the probability distribution of the demon at time t. Similarly, $\boldsymbol{p}^B(t)$ is a vector with two entries, denoting the state of the bit at time t. $\boldsymbol{p}^D_\tau(t_N)$ and $\boldsymbol{p}^B_\tau(t_N)$ are the distributions of the demon and bit at the end of the Nth interval, compared to $\boldsymbol{p}^D_{\rm in}(t_N)$ and $\boldsymbol{p}^B_{\rm in}(t_N)$, which are the distributions at the start of the Nth interval. $\boldsymbol{p}(t)$ is the statistical state of the combined

system with $2k$ entries. Finally, $\boldsymbol{p}_{\rm in}^{D,ps}$ denotes the periodic steady-state distributions at the beginning of each interval of the demon, $\boldsymbol{p}_{\tau}^{D,ps}$ and $\boldsymbol{p}_{\tau}^{B,ps}$ are the periodic steady-state distributions at the end of each interval of the demon and the bit. Here, we stress that the beginning time of the $(N+1)$th interval should be distinguished from the end time of the Nth interval because states of the demon or the bit may undergo abrupt changes due to instantaneous resetting events. In other words, there may be discontinuities of probability states $\boldsymbol{p}^D(t)$ and $\boldsymbol{p}^B(t)$ at $t = t_N$, i.e., $\boldsymbol{p}_{\rm in}^B(t_N) \neq \boldsymbol{p}_{\tau}^B(t_{N-1})$ or $\boldsymbol{p}_{\rm in}^D(t_N) \neq \boldsymbol{p}_{\tau}^D(t_{N-1})$ [without resetting, the equality $\boldsymbol{p}_{\rm in}^D(t_N) = \boldsymbol{p}_{\tau}^D(t_{N-1})$ always holds]. The statistical state of the combined system comprised of the k-state demon and the current bit (with two states 0 or 1) of the tape at the beginning time of the Nth interval is given by the $2k$ dimensional vector

$$\boldsymbol{p}_{\rm in}(t_N) = \mathcal{M}\boldsymbol{p}_{\rm in}^D(t_N), \quad \mathcal{M} = \begin{pmatrix} p_0\mathbb{I} \\ p_1\mathbb{I} \end{pmatrix},$$

where $\mathbb{I}$ is a $k \times k$ identity matrix and $\mathcal{M}$ is a $2k \times k$ matrix denoting a mapping from the demon subspace $(k \times 1)$ to the total combined space $(2k \times 1)$. What is more, through defining some projectors, it would also be easy to extract the distributions in demon subspace and bit subspace from the distributions in the combined space at any time t as follows:

$$\begin{aligned} \boldsymbol{p}^D(t) &= \mathcal{P}^D\boldsymbol{p}(t), \\ \mathcal{P}^D &= (\mathbb{I}, \mathbb{I}), \end{aligned} \tag{1}$$

$$\begin{aligned} \boldsymbol{p}^B(t) &= \mathcal{P}^B\boldsymbol{p}(t), \\ \mathcal{P}^B &\equiv \begin{pmatrix} 1 & \dots & 1 & 0 & \dots & 0 \\ 0 & \dots & 0 & 1 & \dots & 1 \end{pmatrix}_{2\times 2k}, \end{aligned} \tag{2}$$

with $\mathcal{P}^D$ and $\mathcal{P}^B$ denoting the projectors from the combined space to the demon subspace and to the bit subspace respectively. The combined system of the demon and the tape evolves under the master equation

$$\frac{d}{dt}\boldsymbol{p}(t) = \mathcal{R}\boldsymbol{p}(t) \tag{3}$$

during an interval from $t = N\tau$ to $t = (N+1)\tau$, where $\mathcal{R}$ is a $2k \times 2k$ transition matrix whose diagonal elements are $R_{ii} = -\sum_{i\neq j} R_{ji}$, and off-diagonal elements R_{ji} are the transition rates from state i to state j. As a result of the evolution equation (3), the probability distribution of the combined system at the end of the current interval reads $\boldsymbol{p}_{\tau}(t_N) = e^{\mathcal{R}\tau}\boldsymbol{p}(t_N) = e^{\mathcal{R}\tau}\mathcal{M}\boldsymbol{p}^D(t_N)$. Then the corresponding statistical state of the demon can be written as

$$\boldsymbol{p}_{\rm in}^D(t_{N+1}) = \mathcal{T}\boldsymbol{p}_{\rm in}^D(t_N), \quad \mathcal{T} \equiv \mathcal{P}^D e^{\mathcal{R}\tau}\mathcal{M}.$$

We assume that the transition matrix $\mathcal{T}$ is aperiodic and irreducible throughout this work. Then, according to the Perron-Frobenius theorem [51], any initial distribution $\boldsymbol{p}_{{\rm in},0}^D$ at the start of the first interval will evolve asymptotically to a unique periodic steady state $\boldsymbol{p}_{\rm in}^{D,ps}$, which can be obtained by solving the eigenequation of $\mathcal{T}$ corresponding to its largest eigenvalue $\lambda_1 = 1$,

$$\mathcal{T}\boldsymbol{p}_{\rm in}^{D,ps} = \boldsymbol{p}_{\rm in}^{D,ps}, \tag{4}$$

$$\text{with } \boldsymbol{p}_{\rm in}^{D,ps} = \lim_{n\to\infty} \mathcal{T}^n \boldsymbol{p}_{{\rm in},0}^D. \tag{5}$$

This unique periodic steady state is just the functional state of the autonomous Maxwell's demon, which can produce anomalous work stably. To calculate the work produced by the information engine through exploiting the memory tape, Mandal and Jarzynski have defined a quantity named as average production,

$$\Phi(\tau) \equiv p_1^f - p_1 = p_0 - p_0^f, \tag{6}$$

where p_1^f and p_0^f are probabilities of the outgoing bit to be in states 1 and 0 (in the periodic steady state). The values of p_1^f and p_0^f are determined by

$$\boldsymbol{p}_{\tau}^{B,ps} \equiv \begin{pmatrix} p_0^f \\ p_1^f \end{pmatrix} = \mathcal{P}^B e^{\mathcal{R}\tau}\mathcal{M}\boldsymbol{p}_{\rm in}^{D,ps}. \tag{7}$$

Then the average output work per interaction interval can be computed as (in the unit of k_BT)

$$\langle W \rangle = \Phi(\tau) \cdot w,$$

with w being the work done by the combined system when a single jump of the bit from 0 to 1 happens. A positive value of $\langle W \rangle$ implies that the autonomous demon is converting information resources into work.

We employ the simplest two-state demon model, referred to as the information refrigerator, as our primary illustrative example, which is our main focus in this paper. This model involves a demon possessing two energy states, namely, an up state u with energy E_u and a down state d with energy E_d $(E_u > E_d)$. The demon is coupled with a memory tape, resulting in a four-state composite system (see Fig. 1), with two heat baths at different temperatures being the environment. During each interaction interval, when the demon autonomously transitions randomly between its up and down states, with the current bit remaining unchanged, it interacts with the heat bath at a higher temperature T_h. These intrinsic transitions of the demon is irrelevant to bits. Moreover, another kind of cooperative transitions $0d \leftrightarrow 1u$ are allowed. In these transitions, the demon shifts from the down state to the up state only if the current bit undergoes a simultaneous transition from 0 to 1. Conversely, the demon transitions from the up state to the down state when the bit changes from 1 to 0. When these cooperative transitions happen, the demon comes into contact with the heat bath at low temperature T_c. During this interaction, energy is exchanged between the demon and the cold heat bath. All transition rates, whether intrinsic transitions $(R_{d\to u},\ R_{u\to d})$ or cooperative transitions $(R_{0d\to 1u},\ R_{1u\to 0d})$ adhere to the detailed balance conditions as follows:

$$\frac{R_{d\to u}}{R_{u\to d}} = e^{-\beta_h \Delta E}, \quad \frac{R_{0d\to 1u}}{R_{1u\to 0d}} = e^{-\beta_c \Delta E}$$

where $\beta_{h,c} = 1/(k_B T_{h,c})$. For later convenience, we parametrize them as: $R_{d\to u} = \Gamma(1-\sigma)$, $R_{u\to d} = \Gamma(1+\sigma)$, $R_{0d\to 1u} = 1-\omega$, $R_{1u\to 0d} = 1+\omega$. The characteristic transition rate Γ, which quantifies the intrinsic transition rate of the demon is set to be 1 in the rest of the text. Note that Γ can be regarded as the time unit. Here, $0 < \sigma = \tanh(\beta_h \Delta E/2) < 1$ and $0 < \omega = \tanh(\beta_c \Delta E/2) < 1$. We also define

$$\epsilon = \frac{\omega - \sigma}{1 - \omega\sigma} = \tanh\frac{(\beta_c - \beta_h)\Delta E}{2},$$

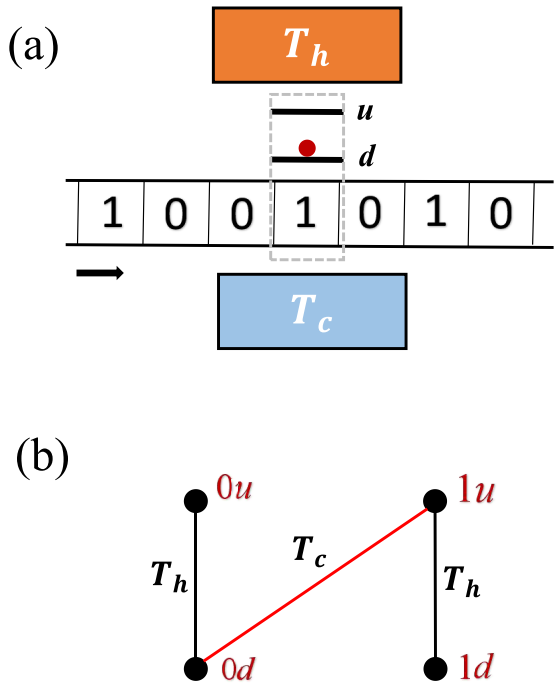

FIG. 1. The information refrigerator model. (a) The two-state demon interacts with a sequence of bits and two reservoir at different temperature. (b) Graph depiction of the composite 4-state system. Nodes denote the combined states and edges denote the allowed transitions, and each pair of transitions satisfies detailed balance conditions. The red edge represents the transition under the low temperature T_c, the other edges correspond to the transition at temperature T_h.

with $0 < \epsilon < \omega$ quantifying the temperature difference between the two reservoirs. It is a central quantity in the studies of thermal machines.

For each interaction interval, if a single bit turns from 0 to 1 due to the cooperative transition, then a fixed amount of energy $\Delta E = E_u - E_d$ is extracted from the cold reservoir, which can be identified as the anomalous work done by the demon. Consequently, the average output work due to the two-state demon in this model reads $\langle W \rangle \equiv Q_{c\to h} = \Phi(\tau) \cdot w = \Phi(\tau)(E_u - E_d)$, where the average production $\Phi(\tau)$ can be computed using Eqs. (3)–(5). More details about this model are described in the Appendix A.

Formalism of discrete-time stochastic resetting. Here we would like to introduce a discrete-time resetting mechanism, which is randomly imposed on the k-state demon at the end of each interaction interval with a probability $\gamma = 1 - e^{-r\tau}$, where r is the resetting rate (a protocol, which may be used to experimentally realized this mechanism is proposed in the Appendix B). Under this setting, the larger the resetting rate r and the time interval τ, the more possible a resetting event will happen. When a resetting event takes place, the demon would be taken to a given state $\mathbf{\Delta}$ instantaneously. Let $\boldsymbol{p}^D_{\text{in},0}$ denote the initial distribution of demon, which is prepared as an equilibrium state by letting the demon be in contact with a thermal reservoir whose temperature is T_{in}. Then, in the absence of resetting, the evolution of the state of demon at the beginning of each interval can be described as

$$\boldsymbol{p}^D_{\text{in}}(t_N) = \mathcal{T}^N \boldsymbol{p}^D_{\text{in},0}. \tag{8}$$

With fixed-rate resetting events all happening at the end of interaction intervals, the demon's evolution reads

$$\boldsymbol{p}^D_{\text{in}}(r, t_N) = e^{-r\tau}\mathcal{T}\boldsymbol{p}^D_{\text{in}}(r, t_{N-1}) + (1 - e^{-r\tau})\mathbf{\Delta}. \tag{9}$$

Thus the demon's initial distribution at time $t = N\tau$ is formally determined by

$$\boldsymbol{p}^D_{\text{in}}(r, t_N) = e^{-rN\tau}\boldsymbol{p}^D_{\text{in}}(t_N) + (1 - e^{-r\tau})\sum_{n=0}^{N-1}[e^{-rn\tau}\mathbf{\Delta}_{n\tau}], \tag{10}$$

where $\mathbf{\Delta}_{n\tau} \equiv \mathcal{T}^n\mathbf{\Delta}$ refers to the state $\mathbf{\Delta}$ evolves to after n intervals. This is a renewal equation connecting the distribution at the beginning of each interval under discrete-time resetting with the distribution under the reset-free dynamics. On the right-hand side of Eq. (10), the first term $e^{-rN\tau}\boldsymbol{p}^D_{\text{in}}(t_N)$ accounts for the situation when there is no resetting events until time $t = N\tau$, the corresponding probability of which is $e^{-rN\tau}$. The nth term in the summation denotes the case in which the last restart happened at time $t = (N - n)\tau$, whose probability is $(1 - e^{-r\tau})e^{-rn\tau}$. The summation of the probabilities of all possible events mentioned above is

$$\begin{aligned} p_{\text{tot}} &= e^{-rN\tau} + (1 - e^{-r\tau})\sum_{n=0}^{N-1} e^{-rn\tau} \\ &= e^{-rN\tau} + 1 - e^{-rN\tau} = 1, \end{aligned}$$

satisfying the normalization condition. Note that when $\tau \to 0$, our renewal equation for discrete-time resetting distribution reduces to the continuous time counterpart as in [34],

$$\boldsymbol{p}^D(r, t) = e^{-rt}\boldsymbol{p}^D(t) + r\int_0^t dt' e^{-rt'}\mathbf{\Delta}_{t'}, \tag{11}$$

because when $\tau \to 0$, one has $(1 - e^{-r\tau}) \to r\tau \equiv r dt'$.

To obtain the whole dynamics with resetting, it would be helpful to utilize the spectral analysis method, solving the eigenvalues problem of the evolution matrix $\mathcal{T}$. The matrix $\mathcal{T}$ has right eigenvectors $\{\boldsymbol{R}_i\}$ and left eigenvectors $\{\boldsymbol{L}_i\}$ satisfy $\mathcal{T}\boldsymbol{R}_i = \lambda_i\boldsymbol{R}_i$ and $\boldsymbol{L}_i^{\mathrm{T}}\mathcal{T} = \lambda_i\boldsymbol{L}_i^{\mathrm{T}}$, with λ_i $(i = 1, 2, ..., k)$ the eigenvalues, which are sorted as $1 = \lambda_1 > |\lambda_2| \geqslant |\lambda_3| \geqslant ... \geqslant |\lambda_k|$ (we assume that λ_2 is nondegenerate). Then according to completeness relation the initial state $\boldsymbol{p}^D_{\text{in},0}$ and resetting state $\mathbf{\Delta}$ can be expanded separately as

$$\begin{aligned} \boldsymbol{p}^D_{\text{in},0} &= \boldsymbol{p}^{D,ps}_{\text{in}} + \sum_{i\geqslant 2}^{k} a_i\boldsymbol{R}_i, \\ \mathbf{\Delta} &= \boldsymbol{p}^{D,ps}_{\text{in}} + \sum_{i\geqslant 2}^{k} d_i\boldsymbol{R}_i. \end{aligned} \tag{12}$$

where $a_i = \frac{\boldsymbol{L}_i^{\mathrm{T}}\cdot\boldsymbol{p}^D_{\text{in},0}}{\boldsymbol{L}_i^{\mathrm{T}}\cdot\boldsymbol{R}_i}$ and $d_i = \frac{\boldsymbol{L}_i^{\mathrm{T}}\cdot\vec{\Delta}}{\boldsymbol{L}_i^{\mathrm{T}}\cdot\boldsymbol{R}_i}$ are coefficients. Thus the state of the demon at the beginning of the Nth time interval can be written as

$$\boldsymbol{p}^D_{\text{in}}(t_N) = \mathcal{T}^N\boldsymbol{p}^D_{\text{in},0} = \boldsymbol{p}^{D,ps}_{\text{in}} + \sum_{i\geqslant 2}^{k} a_i\lambda_i^N\boldsymbol{R}_i, \tag{13}$$

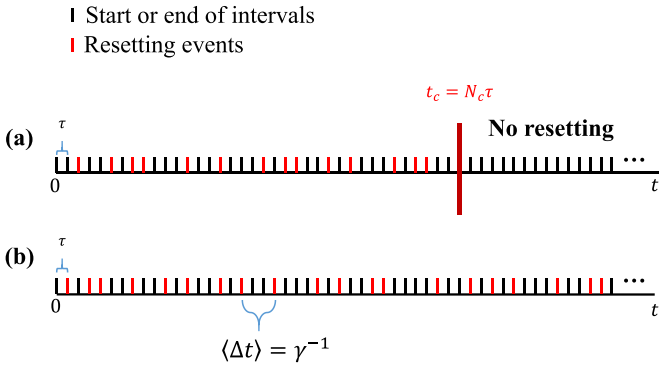

FIG. 2. An illustration of two resetting strategies. (a) The first resetting strategy: closing the reset after a critical time t_c. (b) The second resetting strategy: always keeping the reset on.

and

$$\mathbf{\Delta}_{n\tau} \equiv \mathcal{T}^n \mathbf{\Delta} = \boldsymbol{p}_{\rm in}^{D,ps} + \sum_{i\geqslant 2}^{k} d_i \lambda_i^n \boldsymbol{R}_i. \tag{14}$$

It is worth mentioning that Eq. (13) may be generally used to analyze relaxation processes in other time-periodic or discrete-time Markov systems. One can identify the second term on the right-hand side of Eq. (13) as a slowest decaying mode dominating the relaxation time scale, once the second coefficient a_2 is not equal to zero. In this case, the relaxation timescale is typically characterized by $\tau_{\rm rel} = -1/\ln|\lambda_2|$ (see Appendix C).

To proceed, we describe the two resetting strategies, which we would use to devise the autonomous demon in detail. The first resetting strategy is randomly resetting the demon to the reset state and then switching off the resetting after a given time $t_c = N_c\tau$, causing the system to evolve according to the original dynamics without resetting. The whole dynamics of the first strategy can be formulated as (recall that $\gamma = 1 - e^{-r\tau}$ is the probability that a resetting event happens at the end of an interval)

$$\begin{aligned}\boldsymbol{p}_{\rm in}^{D}(r,t_N) = &\left[\gamma\mathcal{T}\boldsymbol{p}_{\rm in}^{D}(r,t_{N-1}) + (1-\gamma)\vec{\Delta}\right]\Theta(N_c - N)\\ &+ \mathcal{T}\boldsymbol{p}_{\rm in}^{D}(r,t_{N-1})\Theta(N - N_c),\end{aligned} \tag{15}$$

where Θ is the Heaviside step function. The first strategy can be used to eliminate the slowest decaying mode (making $a_2 = 0$) so that the demon would reach its functional state at a greatly faster pace. The second strategy is simply to keep the stochastic resetting mechanism always on so that the combined system will eventually reach a new periodic steady state, whose properties depend on the resetting rate r. For an illustration of the two resetting strategies, see Fig. 2.

Note that the resetting state is chosen to be a single state [e.g., $(0, 1)^{\rm T}$ for the two-state demon] instead of a mixed state in this paper. Physically, resetting the demon to a mixture of states is equivalent to the superposition of the events that demon being reset to different single states with probabilities smaller than one. This may be more challenging to achieve experimentally. Equipped with these discrete-time resetting formalism and the eigenvector-expansion formula, the design principles for autonomous Maxwell's demons are provided in the next two sections.

III. INDUCING FASTER RELAXATION THROUGH RESETTING

In this section, we show how the first resetting strategy accelerate the relaxation from an arbitrary initial distribution to demon's functional steady state significantly. That is, our aim here is to provide a strategy to shorten the warming-up phase of any autonomous information engine. This significantly fast relaxation phenomenon induced by the stochastic resetting is similar to the Markovian Mpemba effect [46,48–50]. To eliminate the slowest decaying mode of the system (so that it would not be trapped in a metastable state), we just need to turn off the resetting mechanism at a critical time $t_c = N_c\tau$, after which the demon system will relax freely obeying the original evolutionary dynamics (8) with the coefficient of the relaxation mode (ith coefficient of the eigenvector expansion) $\boldsymbol{R}_i$ being $a_i(r, N_c)$. Under this protocol, one can conveniently modify the value of $a_2(r, N_c)$, the coefficient of the slowest decaying mode in the free relaxation process, through controlling the value of r and N_c. Plugging (13) and (14) into Eq. (10) one can obtain (see Appendix B for details)

$$\boldsymbol{p}_{\rm in}^{D}(r,t_N) = \boldsymbol{p}_{\rm in}^{D,ps} + \sum_{i\geqslant 2}^{k} a_i(r,N)\lambda_i^N \boldsymbol{R}_i, \tag{16}$$

where the modified ith coefficient at Nth interaction interval $a_i(r, N)$ reads

$$a_i(r,N) = \left[a_i - \frac{d_i(1-e^{-r\tau})}{1-\lambda_i e^{-r\tau}}\right]e^{-rN\tau} + \frac{d_i(1-e^{-r\tau})}{1-\lambda_i e^{-r\tau}}\cdot\lambda_i^{-N}. \tag{17}$$

Here d_i is the ith coefficient of the expanded form of the $\vec{\Delta}$, depending on the choice of the reset state. Therefore, the whole dynamics under the first resetting strategy obeys

$$\begin{aligned}\boldsymbol{p}_{\rm in}^{D}(r,t_N) &= \boldsymbol{p}_{\rm in}^{D,ps} + \sum_{i\geqslant 2}^{k} a_i(r,N)\lambda_i^N \boldsymbol{R}_i \quad N \leqslant N_c,\\ \boldsymbol{p}_{\rm in}^{D}(r,t_N) &= \boldsymbol{p}_{\rm in}^{D,ps} + \sum_{i\geqslant 2}^{k} a_i(r,N_c)\lambda_i^N \boldsymbol{R}_i \quad N > N_c.\end{aligned} \tag{18}$$

By closing the reset at an appropriate critical time t_c, one can make the second coefficient being zero so that the relaxation gets accelerated to the maximum extent, corresponding to the so-called "strong" Mpemba effect. That is, the crucial condition to realize significantly fast relaxation is given by

$$a_2(r,N) = 0, \tag{19}$$

from which the appropriate time to close the reset can be obtained as shown below. Combining Eq. (19) with Eq. (17) one gets the appropriate critical number of interaction intervals if the second eigenvalue $\lambda_2 > 0$,

$$N_c = \frac{1}{r\tau - \ln\lambda_2}\ln\left[1 - \frac{a_2}{d_2}\frac{1-\lambda_2 e^{-r\tau}}{1-e^{-r\tau}}\right], \tag{20}$$

which is our first main result. From the expression of N_c we clearly see that the sufficient condition for the existence of

a physical critical number $N_c \geqslant 1$ is just $a_2/d_2 \leqslant 0$ (when $a_2/d_2 > 0$, one may still find $N_c \geqslant 1$ by making $r\tau - \ln\lambda_2 < 0$), since the right-hand side is a decreasing function of $r\tau$ that can sweep the full interval $(0, \infty)$ when $r\tau \geqslant \ln\lambda_2$. The calculated N_c may not be an integer, which is forbidden in our setting. However, one can always make N_c be an integer by controlling the value of r. Furthermore, we expect to make N_c be a small positive number (like the smallest positive integer, one) through modifying the resetting rate r whenever the condition $a_2/d_2 \leqslant 0$ is fulfilled, thus the resetting strategy could always significantly reduce the total time cost to demon's functional state compared to the reset-free dynamics.

Besides, when $\lambda_2 < 0$, one can still tune the resetting rate r to let $N_c = 1$ in the region $a_2/d_2 \geqslant 0$. In this case, the value of N_c should be obtained by solving the self-consistent equation

$$N_c = \frac{1}{r\tau - \ln|\lambda_2|} \ln\left[(-1)^{N_c}\left(1 - \frac{a_2}{d_2}\frac{1-\lambda_2 e^{-r\tau}}{1-e^{-r\tau}}\right)\right], \quad (21)$$

which does not have a closed-form solution. But when N_c is given, one can use the equation to obtain the corresponding value of r that can realized the desired N_c. For instance, if we want N_c to be 1, we can tune the resetting rate r to make the equation

$$N_c = \frac{1}{r\tau - \ln|\lambda_2|} \ln\left[\frac{a_2}{d_2}\frac{1-\lambda_2 e^{-r\tau}}{1-e^{-r\tau}} - 1\right]$$

hold (when $a_2/d_2 \geqslant 1$ the r always exists).

To illustrate how the above strategy can be utilized to improve the performance of autonomous Maxwell's demon, we focus on a specific model, the two-state information refrigerator mentioned above. In this model, we always have $\lambda_2 > 0$ when $\delta \geqslant 0$ (see Appendix D).

For the two-state information refrigerator, the resetting state could be $\vec{\Delta}_d = (0,1)^{\mathrm{T}}$ or $\vec{\Delta}_u = (1,0)^{\mathrm{T}}$, we choose the former one. Initially, we let the two-state demon be in contact with a heat bath whose temperature is T_{in} for long enough time so that the demon reaches the thermal equilibrium. Then the initial distribution of the two-state demon is just

$$\boldsymbol{p}^D_{\mathrm{in},0} = \left(\frac{e^{-\Delta E/T_{\mathrm{in}}}}{1+e^{-\Delta E/T_{\mathrm{in}}}}, \frac{1}{1+e^{-\Delta E/T_{\mathrm{in}}}}\right)^{\mathrm{T}}, \quad (22)$$

which makes the second coefficient $a_2(T_{\mathrm{in}})$ be a function of the initial temperature, so is the modified second coefficient $a_2(r, N, T_{\mathrm{in}})$. It is clear from Eq. (20) that once the initial temperature allows the critical interaction number to be positive, then one can always make N_c the smallest positive integer 1 by virtue of adjusting the resetting constant r, whatever the dynamical details (i.e., values of $\delta = p_0 - p_1$ and the temperature difference quantifier ϵ of the two heat baths) of the system is. Note that for the information refrigerator system, there is only one right eigenvector $\boldsymbol{R}_2$ as the relaxation mode apart from the stationary distribution, i.e.,

$$\boldsymbol{p}^D(r, t_N) = \boldsymbol{p}^{D,ps}_{\mathrm{in}} + a_2(r, N, T_{\mathrm{in}})\lambda_2^N \boldsymbol{R}_2.$$

In result, $a_2(r, N_c, T_{\mathrm{in}}) = 0$ signifies the arrival of the functional periodic steady state $\boldsymbol{p}^{D,ps}_{\mathrm{in}}$. Thus for the two-state demon one can invariably expect the shortest time $t_c = \tau$ to enter the functional state through controlling the resetting parameter r. It should be noted that in our setting, the time for the demon to reach its functional state can never be smaller than τ (one interaction interval), which is the smallest time unit for demon's performance. Therefore, the optimal value of the resetting rate r to make the critical time t_c shortest in this case is obtained by solving the equation $N_c = 1$ when other dynamical parameters are fixed, with the expression of N_c given by Eq. (20). Here, $a_2 = \frac{\boldsymbol{L}_2^{\mathrm{T}}\cdot\boldsymbol{p}^D_{\mathrm{in},0}}{\boldsymbol{L}_2^{\mathrm{T}}\cdot\boldsymbol{R}_2}$, $d_2 = \frac{\boldsymbol{L}_2^{\mathrm{T}}\cdot\boldsymbol{\Delta}}{\boldsymbol{L}_2^{\mathrm{T}}\cdot\boldsymbol{R}_2}$ and λ_2 can be figured out by the spectral analysis of the matrix $\mathcal{T}$. In Fig. 3 we build a phase diagram for the dynamical behavior of the information engine before reaching its functional state. The blue area of the phase diagram corresponds to the fast relaxation ($a_2/d_2 \leqslant 0$) region, where an optimal resetting rate that can lead to the smallest time cost $t_c = \tau$ always exists. This diagram provides guidance to prepare the initial state of the demon to be in an appropriate temperature. What is more, if we set the up state as the reset state, the yellow area in the current diagram would turn to be the efficacious region of resetting. The asymmetry of the efficacious region between up state and down state arises from the energy difference between two states. Then, to illustrate the accelerating effect of stochastic resetting, we further fix the dynamical parameters as $\omega = 1/2$, $\delta = 0.5$, $\epsilon = 0.2$ and prepare the demon initially at $\beta_{\mathrm{in}} = 0.1$, then numerically gives several dynamical trajectories of the probability of the up state $p_u(t)$ under different resetting rates, as plotted in Fig. 4. Note that the resetting dynamics is switched off after a given critical time $t_c(r) = N_c(r)\tau$, depending on the resetting rate r. The optimal value of r, which can make $t_c = \tau$ is also a threshold value. It is shown in Fig. 4 that when the resetting rate r is

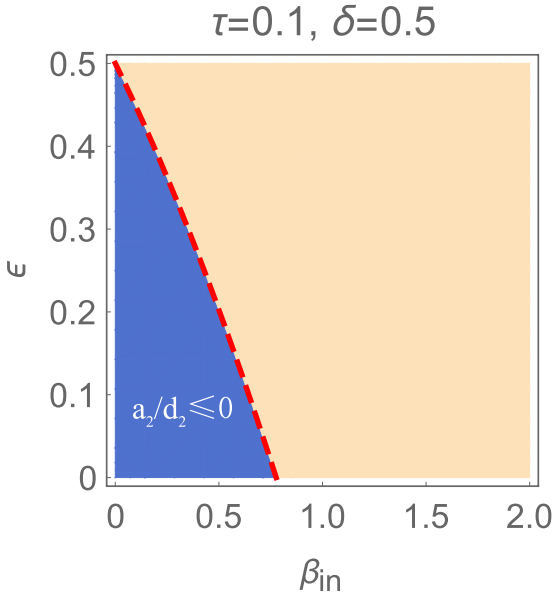

FIG. 3. The phase diagram for the relaxation behavior of the information refrigerator. The parameter is set as $\tau = 0.1, \omega = 1/2, \delta = 0.5$, $\Delta E = 1$ and the reset state is the down state. The blue part is the fast relaxation region ($a_2/d_2 \leqslant 0$), where the demon can reach the functional state significantly faster by stochastic resetting with appropriate rate. The yellow part is the dud region where resetting cannot take effect. However, when the reset state is set to the up state, the yellow region becomes the useful region, while the blue region becomes the useless region. In the red dash line, $a_2 = 0$.

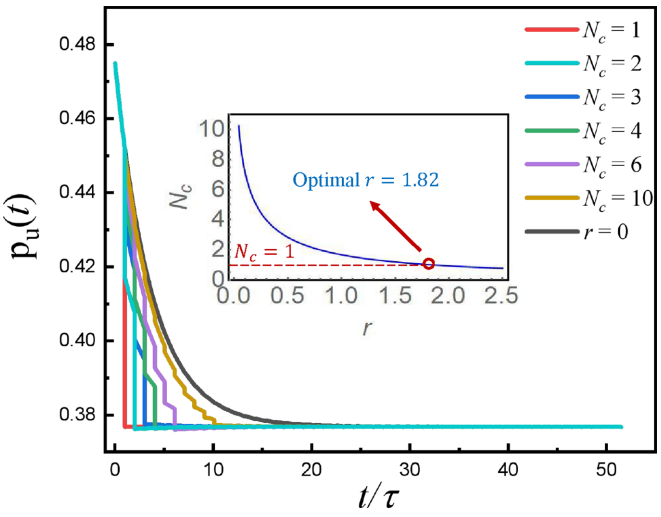

FIG. 4. The evolution of the demon's state under different resetting dynamics. For each dynamics with different resetting rate r, the resetting is closed right after the critical time $t_c(r) = N_c(r)\tau$. We take the dynamics of probability of the up state as an illustration. The dynamical parameters are given by $\tau = 0.1$, $\delta = 0.5$, $\epsilon = 0.2$, and $\beta_{\text{in}} = 0.1$. The inset shows the relation between the critical number N_c and the resetting rate r, and the optimal resetting rate $r = 1.82$ is marked by a red circle in the inset. When $r > 1.82$, the resulting $N_c < 1$ cannot be realized since N_c should be a positive integer.

below this threshold value, the larger the r is, the sooner the refrigerator could get to its functional periodic steady state. However, when the resetting rate is made to be larger than the optimal value, the time cost would become greater than τ. In the limiting case of $r \to \infty$, the demon would be reset to the down state (which can never be the functional state) with probability 1 at the end of each interval, making the critical time t_c go to zero, which is the same as the reset-free dynamics. Under current conditions, the threshold value of r (the optimal r) turns to be 1.82, which is obtained by solving the equation $N_c(r) = 1$. It should be noted that when $r > 1.82$ one has $N_c(r) < 1$, but it cannot be realized. To make it clearer, we plot the relation between the critical number N_c and resetting rate r in the inset of Fig. 4, with the parameters being fixed at the same values as above.

Further, to better illustrate our first strategy that can shorten the warming-up phase of information engines, we provide another example in Appendix E, i,e., a modified three-state information engine introduced in Ref. [43].

We should note that the tailored relaxation time may be worse than the original relaxation time scale $\tau_{\text{rel}} \sim -1/\ln|\lambda_2|$. However, one can guarantee that $N_c\tau < \tau_{\text{rel}}$ through tuning the value of r, so for the two-state demon in which the relaxation time equals $N_c\tau$, the tailored relaxation time can be assured to be shorter than the original one. For general cases, we assume that there is a gap between λ_2 and λ_3, in which case the original process can be significantly accelerated by the first resetting strategy.

At the close of this section, we would like to discuss the connection between the first resetting strategy and the Mpemba effect for completeness. In the relaxation process of a given system, it may be trapped in a metastable state, which is characterized by the dominant eigenmode (i.e., the slowest decaying mode) of the system corresponding to the second largest eigenvalue (e.g., λ_2 in our information refrigerator system) of the transition matrix [see Eq. (13) for better understanding. Here $a_2\lambda_2^n \boldsymbol{R}_2$ is the dominant eigenmode]. Therefore, the relaxation time scale is mainly determined by the spectral gap of the transition matrix, having assumed that λ_2 is unique, i.e., $\lambda_2 > \lambda_3$. Based on the above arguments, Z. Lu and O. Raz have proposed a possible mechanism to explain (in Markovian systems) the Mpemba effect that a system can cool down faster at high temperature than at lower temperature under certain conditions, since the Mpemba effect can be regarded as the effect of initial conditions (initial temperature) on the thermal relaxation processes [48]. The key point is that the coefficient $a_2 = \frac{\boldsymbol{L}_2^{\text{T}} \cdot \boldsymbol{p}_{\text{in},0}^D}{\boldsymbol{L}_2^{\text{T}} \cdot \boldsymbol{R}_2}$ of the dominant eigenmode depends on initial conditions of the system of interest. This coefficient quantifies the degree of overlapping between the initial state $\boldsymbol{p}_{\text{in},0}^D$ and the dominant eigenmode, so that the smaller the $|a_2|$ is, the less likely that the system will be stuck in the metastable state, i.e., will relax faster. As a consequence, if $|a_2|$ turns out to be a nonmonotonic function of the initial temperature T_{in}, the Mpemba effect could happen within a certain temperature range where $|a_2|$ is a decreasing function of temperature. Within this range, the system at higher temperature is initially farther away from the target state with low temperature, but it has more chances to avoid being trapped in the metastable state compared to the same system at lower temperature (still higher than the temperature of the target state). When $|a_2|$ equals to zero at some temperature, the strong Mpemba effect could happen [46].

In our case, the first resetting strategy can tune the value of a_2 as in Eq. (17). By controlling the critical time $t_c = N_c\tau$ to close the reset and the resetting rate r, the fixed value of a_2 [i.e., $a_2(r, N_c)$] after closing the reset can be made to be any value no matter what the initial state is. Therefore, the Mpemba effect or even the strong Mpemba effect is able to be induced by the first resetting strategy through the control of N_c and r. Our first resetting strategy can be optimal over other possible accelerating approaches for the information refrigerator system, since there is only one eigenmode in this system, and it can be eliminated at the fastest pace (N_c can always made to be 1) by the strategy. For the demon with more than two states, there may be some other protocols can eliminate more eigenmodes (simultaneously making $a_2 = 0$, $a_3 = 0$,...), such as the temperature protocol in the reference [45]. However, these protocols are usually more complex than our resetting strategy, which is convenient to realize.

IV. AUTONOMOUS DEMON WITH RESETTING

In this section, we focus on the second resetting strategy, exploring the second dimension of the demon's performance: its effective working range. To study the effective working range of the demon, we first need to analyze the functional state performance of the autonomous demon with the second strategy being imposed on it.

There are two pivotal facets of the functional state performance of the autonomous demon, including the average work production Φ per cycle and the information erasing capability

quantified by the reduction in Shannon entropy of bit per cycle. If the autonomous demon is always under resetting, it eventually converges to a new periodic steady state in the large time limit (the number of interactions $N \to \infty$), which is given by (see Appendix B for details)

$$\boldsymbol{p}_{\rm in}^{D,ps}(r) = \boldsymbol{p}_{\rm in}^{D,ps} + \sum_{i\geqslant 2} \frac{1-e^{-r\tau}}{1-\lambda_i e^{-r\tau}} d_i \boldsymbol{R}_i. \tag{23}$$

As a consequence, the marginal distribution of the outgoing bit in the new periodic steady state can be written as

$$\mathcal{P}_{\tau}^{B,ps}(r) = \mathcal{P}^B e^{\mathcal{R}\tau} \mathcal{M} \boldsymbol{p}_{\rm in}^{D,ps}(r) = \left(p_0^r, p_1^r\right)^{\rm T}. \tag{24}$$

Then, we would like to quantify the two important properties mentioned above in this new functional state, i.e., the average work production and the information erasing capability of the demon, so that the efficacious region could be analyzed in detail. In what follow, the properties of the new functional state are our main focus. Therefore, in the remaining part of this section, we assume the demon has reached its new functional periodic steady state. For simplicity, we take the two-state Maxwell's refrigerator model as an illustrative example. The distribution of demon at the start of each interval is

$$\boldsymbol{p}_{\rm in}^{D,ps}(r) = \boldsymbol{p}_{\rm in}^{D,ps} + \frac{1-e^{-r\tau}}{1-\lambda_2 e^{-r\tau}} d_2 \boldsymbol{R}_2.$$

The performance of the information refrigerator with resetting can be evaluated by the average production of 1's per interaction interval, recalling that the initial distribution of the bit is given by $\boldsymbol{p}_{\rm in}^{B} = (p_0, p_1)^T$,

$$\Phi_{\rm tot}(r,\tau) \equiv p_1^r - p_1 = p_0 - p_0^r. \tag{25}$$

The average transfer of energy from the cold to the hot reservoir is $Q_{c\to h} = \Phi_{\rm tot}\Delta E = \Phi_{\rm tot}(E_u - E_d)$. The total average production per interaction interval is given by

$$\begin{aligned}\Phi_{\rm tot} &= \left(\left[\mathcal{T}' \boldsymbol{p}_{\rm in}^{D,ps}\right]_2 - p_1\right) + \frac{1-e^{-r\tau}}{1-\lambda_2 e^{-r\tau}} d_2 [\mathcal{T}' \boldsymbol{R}_2]_2 \\ &\equiv \Phi_0 + \Phi_r \end{aligned} \tag{26}$$

where $\mathcal{T}' = \mathcal{P}^B e^{\mathcal{R}\tau}\mathcal{M}$. It has been shown that the contribution $\Phi_0 = \Phi_{\rm tot}|_{r=0}$ when there is no reset is (see Appendix A for details)

$$\Phi_0 \equiv \left[\mathcal{T}' \boldsymbol{p}_{\rm in}^{D,ps}\right]_2 - p_1 = \frac{\delta - \epsilon}{2}\eta(\Lambda), \tag{27}$$

where $\eta(\Lambda)$ is a positive function of all the dynamical parameters. Thus we just need to compute the contribution Φ_r arising from stochastic reset. The second right eigenvector is obtained as $\boldsymbol{R}_2 = (1,-1)^T$. We set the resetting state as $\vec{\Delta} = (0,1)^T$ (down state) or $\vec{\Delta} = (1,0)^T$ (up state), and study their contributions respectively. When the demon is reset to the up state, we find that the contribution Φ_r always takes negative value whatever the value of r is. This implies that the up state is not a good choice for the reset state because resetting the demon to up state only has negative impact on the engine's performance, i.e., shrinking the refrigerator region. We will see that the down state $\vec{\Delta} = (0,1)^T$ would be an appropriate option for the demon to be reset to, even might be optimal.

Now consider another important feature of performance of the refrigerator in the new functional state, the information-processing capability of the demon. To quantify the capability, the Shannon entropy difference between the outgoing bit and the incoming bit is introduced as

$$\begin{aligned}\Delta S_B &= S\left(\boldsymbol{p}_{\tau}^{B,ps}\right) - S\left(\boldsymbol{p}_{\rm in}^{B,ps}\right) = S(\delta - 2\Phi_{\rm tot}) - S(\delta), \\ S(\delta) &\equiv -\sum_{i=1}^{1} p_i \ln p_i \\ &= -\frac{1-\delta}{2}\ln\frac{1-\delta}{2} - \frac{1+\delta}{2}\ln\frac{1+\delta}{2}, \end{aligned} \tag{28}$$

which is a measure of how much information content contained in the memory tape is changed due to the demon during each interaction interval. To illustrate the relation between the tape and the value of its Shannon entropy more clearly, we take two specific cases $\delta = \pm 1$ as examples. In these cases $S(\boldsymbol{p}_{\rm in}^{B,ps}) = 0$, which means that all bits in the memory tape are 0 (or 1). When $\delta = 1$, all bits in the memory tape are 0, in which case the amount of information resource is maximal as mentioned in Sec. II. The number of "1" in the tape will always increase, following the positive output of work on average. On the other hand, when $\delta = -1$, all bits in the tape are 1, so that the demon will be useless in this case. This is because the total number of "1" in the tape will always decrease, making the output work negative on average. The information entropy will increase simultaneously, so the demon cannot serve as an eraser either.

Finally, to illustrate the extended effective region of the refrigerator, we fix $\Gamma = 1$, $\omega = 1/2$, $\tau = 1$ and construct several phase diagrams for the refrigerator under different resetting rate r, traversing the parameter space of (δ, ϵ) (Fig. 5). Note that to assure $\beta_c > \beta_h > 0$, parameter ϵ can only range from 0 to 1/2, since we have set $\omega = \tanh(\beta_c \Delta E/2) = 1/2 > \epsilon = \tanh[(\beta_c - \beta_h)\Delta E/2]$. The newly constructed phase diagrams exhibit four distinct regions (excluding the case of $r = 0$, which only has three regions), constituting our second main result. The purple areas are identified as regions representing the information refrigerator, as clearly extended in Figs. 5(b)–5(d) when compared to the initial reset-free demon scenario depicted in Fig. 5(a). This expansion is attributed to the positive contribution Φ_r from resetting, which, in turn, augments the output power. The green parts denote the information eraser regions, where the information stored in the memory tape can be effectively obliterated, restoring a low-information-entropy state that serves as a source for anomalous work. Impressively, the red parts represent dual-function regions where the information machine can simultaneously generate anomalous work and replenish some information resources. The remaining white parts within the phase diagrams are designated as dud regions, wherein the demon lacks the capability to either produce work or erase information from the memory tape, rendering it nonfunctional within this parameter space.

Generalized second law in the presence of resetting. The dual-function region in the new phase diagram shows that the autonomous demon with resetting seems to be against the second law of thermodynamics. To address this issue, a generalized second law is derived by constructing a Lyapunov

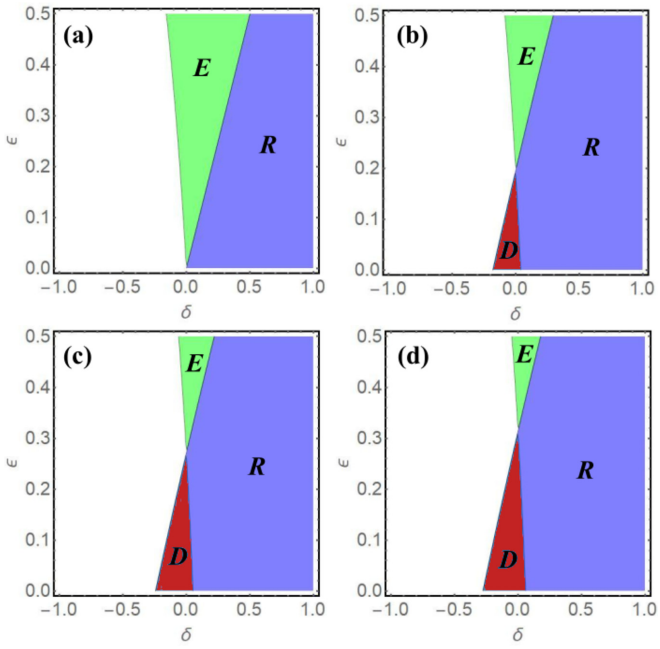

FIG. 5. The new phase diagrams for the demon under different resetting rate r. (a) $r = 0$, not reset. (b) $r = 1$, (c) $r = 2$, (d) $r = 5$. For (a)–(d), interaction interval $\tau = 1$. In all of the diagrams, the green region is the information-eraser region (denoting as "E"), in which the demon is able to reduce the information entropy of the memory tape. The purple region is the refrigerator region (denoting as "R"), where the demon can help to produce anomalous work by exploiting information. The purple region does not exist when $r = 0$. The red region is a dual-function region (denoting as "D"), both of the information erasing and anomalous work production functions could be realized in this region. The white part is the dud region where the demon becomes useless.

function, or by using the integral fluctuation theorem for stochastic entropy production (see Appendix F for details).

As a result, the generalized second law of thermodynamics of the system with resetting in the periodic steady state is demonstrated to be

$$Q_{c\to h}(\beta_h - \beta_c) + \Delta S_B + \Delta S^{\rm rst} \geqslant 0. \tag{29}$$

This generalized second law is our third main result. The new term $\Delta S^{\rm rst}$ is the entropic cost for resetting [39] during an interval $[n\tau, (n+1)\tau]$, and for the information refrigerator it is given by

$$\Delta S^{\rm rst} = \Delta S_D + \beta_h \Delta p^{D,ps} \Delta E. \tag{30}$$

Here, $\Delta p^{D,ps} \equiv p^{D,ps}_{\tau,u} - p^{D,ps}_{{\rm in},u}$ denotes the difference between the steady-state probability of the demon in up state at the final moment and at the initial moment within an interval. From the expression, we can see that this new term contributed by resetting consists of two parts. The first part is the Shannon entropy difference between the initial distribution and the final distribution in each interaction interval, which is the system entropic change due to resetting. The second part $\beta_h \Delta p^{D,ps} \Delta E$ can be interpreted as the entropic flux associated with the energy cost (heat flow) needed to maintain this distribution difference between the demon at the final moment and at the initial moment, or say, to maintain the new

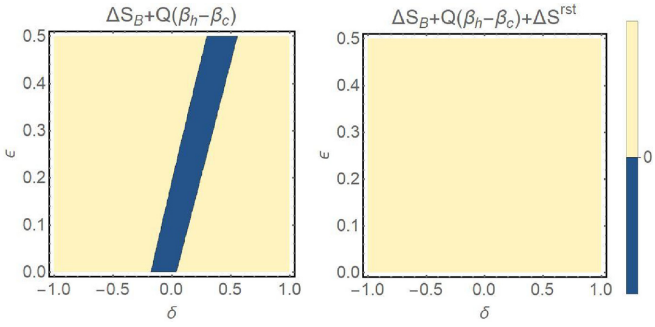

FIG. 6. Apparent violation and restoration of the second law of thermodynamics in the information refrigerator system for $\tau = 1.0$. (a) The apparent violation of the original modified second law of thermodynamics. (b) A demonstration of the generalized second law incorporating the contribution from stochastic reset.

periodic steady state. To demonstrate the generalized second law, we plot two plots for the signs of $Q_{c\to h}(\beta_h - \beta_c) + \Delta S_B$ and $Q_{c\to h}(\beta_h - \beta_c) + \Delta S_B + \Delta S^{\rm rst}$ respectively as functions of ϵ and δ in the Fig. 6 (contour plot of the detailed values of these two functions are given at the end of the Appendix E for completeness). The plots contain distinct regions, with the yellow regions representing positive values of the plotted function and the blue regions indicating negative values. Figure 6(a) shows that there is a parameter region where $Q_{c\to h}(\beta_h - \beta_c) + \Delta S_B < 0$, so the original second law derived by Mandal and Jarzynski is violated in this region. It is worth noting that this region where second law is apparently violated is larger than the dual function region shown in Fig. 5(b). This is because there is a parameter region in which ΔS_B satisfies $0 < \Delta S_B < Q_{c\to h}(\beta_c - \beta_h)$. This region, which satisfies this condition, belongs to the refrigerator region, and the original second law is simultaneously violated within it. The restoration of the second law after considering the effect of stochastic reset is demonstrated in Fig. 6(b), thereby validating the generalized second law Eq. (29). The generalized second law for the demon with more states can also be found in a similar manner. What is more, employing the so-called thermodynamic uncertainty relation (TUR) [52–56] may yield a relation stronger than the generalized second law (29). This could be left for the future study.

Based on the expression (30) we may explain physically why the down state $\vec{\Delta} = (0, 1)^{\rm T}$ should be chosen as the resetting state to improve the engine's performance, instead of the up state $\vec{\Delta} = (1, 0)^{\rm T}$ or any mixed state. Actually, the down state may be the optimal option for optimizing the performance of the information refrigerator. To improve the overall performance of the information refrigerator, a larger cost from resetting $\Delta S^{\rm rst}$ is preferred. This is because a larger cost leads to a greater anomalous energy transfer $Q_{c\to h}$ and a smaller the entropy difference ΔS_B. Therefore, the optimal resetting mechanism should maximize the $\Delta p^{D,ps}$ and the ΔS_D simultaneously. If the demon is reset to a given mixed state like $(1/2, 1/2)^{\rm T}$, the initial Shannon entropy $S_{D,0}$ would take the maximal value, resulting in $\Delta S_D < 0$. In contrast, resetting the demon to a single state like $(0, 1)^{\rm T}$ or $(1, 0)^{\rm T}$ would make the Shannon entropy of the demon at the initial moment of an interval being zero, always following with

$\Delta S_D > 0$. Thus resetting the demon to a single state could be superior to resetting it to a mixed state. On the other hand, if the demon is reset to the up state at the end of each interval, the probability of it being in up state initially turns to be 1, leading $\Delta p^{D,ps}$ to equals $p^{D,ps}_{\tau,u} - 1 < 0$, which has a negative impact on the refrigerator's performance. Contrarily, the down-state reset continues to have a positive effect on this term as $\Delta p^{D,ps} = p^{D,ps}_{\tau,u} > 0$. In consequence, picking the down state $(0, 1)^{\mathrm{T}}$ as the reset state rather than other states appears to be the optimal strategy.

To conclude this section, we would like to discuss the four regions in the new phase diagram according to Eq. (26) and the generalized second law Eq. (29). When $\delta > \epsilon$, the driving from the incoming 0 bit prevails over the temperature difference of two heat baths, so that the demon generates heat flow from the cold bath to the hot bath even in the $r = 0$ case as in Fig. 5(a), since $\Phi_0 > 0$. The borderline between the refrigerator region and the eraser region here is the $\delta = \epsilon$ line. When $\delta < \epsilon$, the driving from the memory tape cannot overcome the temperature difference ($\Phi_0 < 0$), however, the positive contribution Φ_r from reset can make the total average production $\Phi_{\mathrm{tot}} = \Phi_0 + \Phi_r > 0$ in some parameter intervals, resulting in the extension of the refrigerator region [the borderline moves from $\delta = \epsilon$ to the left as in Figs. 5(b)–5(d)]. When $r > 0$, a dual-function region emerges to the left of the boundary between the dud region and the eraser region in the $r = 0$ case. The dual-function region arises from the positive contribution ΔS^{rst}. The dual-function region is always inside the dud region of the reset-free case, so the effective working region of the demon with resetting is always larger than that of the original demon.

V. DISCUSSION

Autonomous Maxwell's demons have garnered significant attention in the field of small-system thermodynamics since Mandal and Jarzynski proposed their exactly solvable model in 2012. An intriguing facet of this model is that the evolution of the memory tape is subject to periodic resetting—a mechanism wherein the tape's state is consistently returned to an given state after fixed time intervals τ. This consistent resetting of the memory tape prompts an intriguing question: What if we expose the demon to resetting, akin to the bit's dynamics? Such an approach could potentially enhance the demon's performance. Indeed, research has demonstrated that resetting protocol can be devised to optimize various dynamical processes [34,41,42]. Consequently, the idea of random resets for the demon holds significant promise. However, most existing frameworks of stochastic resetting only deal with the continuous-time Markov process. These frameworks may not directly apply to our scenario, where demon resets are expected to occur only at the conclusion of specific interaction intervals.

In this article, we generalize the stochastic resetting formalism to discrete-time Markov process. This allows us to introduce this mechanism to autonomous Maxwell's demon systems, providing design principles and strategies. Moreover, we also report tools for analytically analyzing the relaxation process in time-periodic or discrete-time Markov systems, as in Eq. (13). Equipped with these tools, we have systematically studied the effect of stochastic reset on the demon system. To begin, we study the time cost for the autonomous demon to relax to its working state (the periodic steady state), which has not been taken into account in previous studies [8,10,15]. This is an important consideration in real systems, as minimizing the time cost for relaxation processes is desirable. Using stochastic resetting, we provide design principles to optimize this relaxation process, minimizing the time cost to enter the working state through a protocol inspired by the strong Mpemba effect. Furthermore, we construct functional states with remarkable features by keeping resetting the demon. We also derive a generalized second law of thermodynamics that takes the contribution from discrete-time stochastic reset into account. We believe that our paper provides insights into the role of stochastic resetting in autonomous demon systems. Our results could be used to design more efficient and effective demon systems.

An intriguing open problem lies in the extension of our framework to accommodate time-dependent resetting rates, where the waiting time distribution between consecutive resetting events deviates from the exponential distribution. The exploration of alternative waiting time distributions that could potentially enhance the performance of autonomous demons remains a compelling avenue for future research. Furthermore, the concept of stochastic resetting has recently piqued significant interest in the realm of quantum systems [57,58]. Thus, it would be promising to develop a framework as the quantum counterpart of our discrete-time resetting framework. Such a framework could prove invaluable in analyzing resetting mechanisms within the domain of quantum systems, marking a fruitful direction for further investigation.

ACKNOWLEDGMENTS

This work is supported by MOST (Grant No. 2022YFA1303100) and NSFC (Grant No. 32090044).

APPENDIX A: DETAILS OF INFORMATION REFRIGERATOR

Extra details of the original information refrigerator. The transition matrix of the four-state combined system in this model is given by

$$\mathcal{R} = \begin{pmatrix} -\Gamma(1+\sigma) & \Gamma(1-\sigma) & 0 & 0 \\ \Gamma(1+\sigma) & -[1-\omega+\Gamma(1-\sigma)] & 1+\omega & 0 \\ 0 & 1-\omega & -[1+\omega+\Gamma(1+\sigma)] & \Gamma(1-\sigma) \\ 0 & 0 & \Gamma(1+\sigma) & -\Gamma(1-\sigma) \end{pmatrix}.$$

Solution to the periodic steady state the expression of average production is as follows: the evolution matrix for initial distribution of the demon is given by

$$\mathcal{T} = \mathcal{P}^D e^{\mathcal{R}\tau}\mathcal{M},\ \mathcal{P}^D = \begin{pmatrix} 1 & 0 & 1 & 0 \\ 0 & 1 & 0 & 1 \end{pmatrix},$$

$$\mathcal{M} = \begin{pmatrix} p_0 & 0 \\ 0 & p_0 \\ p_1 & 0 \\ 0 & p_1 \end{pmatrix}.$$

Then the periodic steady state $\boldsymbol{p}_{\rm in}^{D,ps}$ for demon can be obtained by solving the linear equation

$$\mathcal{T}\boldsymbol{p}_{\rm in}^{D,ps} = \boldsymbol{p}_{\rm in}^{D,ps}.$$

In the periodic steady state, the joint distribution of the demon and the interacting bit, at the end of the interaction interval, is given by $\boldsymbol{p}_\tau^{ps} = e^{\mathcal{R}\tau}\mathcal{M}\boldsymbol{p}_{\rm in}^{D,ps}$. The marginal distribution of the outgoing bit is then given by projecting out the state of the demon,

$$\boldsymbol{p}_\tau^{B,ps} = (p_0^f, p_1^f) = \mathcal{P}^B e^{\mathcal{R}\tau}\mathcal{M}\boldsymbol{p}_{\rm in}^D, \mathcal{P}^B = \begin{pmatrix} 1 & 1 & 0 & 0 \\ 0 & 0 & 1 & 1 \end{pmatrix}. \tag{A1}$$

Notice that $\boldsymbol{p}_{\rm in}^{D,ps}$ is the first right eigenvector of $\mathcal{T}$, $\boldsymbol{p}_\tau^{B,ps} = (p_0^f, p_1^f)$ then can be solved, which determines the value of average production as $\Phi = p_1^f - p_1$. By performing these calculations using Mathematica,

$$\Phi = \frac{\delta - \epsilon}{2}\eta(\Lambda),\ \eta(\Lambda) = \frac{\nu_2 P + \nu_3 Q}{P + Q}, \tag{A2}$$

$$P = \mu_2(\mu_4\nu_3 + \mu_1\nu_1), Q = \mu_3(\mu_4\nu_2 + \mu_1\nu_1), \tag{A3}$$

where

$$\nu_1 = 1 - e^{-2\Gamma\tau}, \nu_2 = 1 - e^{-(1+\Gamma-\alpha)\tau}, \nu_2 = 1 - e^{-(1+\Gamma+\alpha)\tau}, \tag{A4}$$

$$\mu_1 = (\delta + \sigma)\omega, \mu_2 = \alpha + \Gamma + \sigma\omega, \mu_3 = \alpha - \Gamma - \sigma\omega,$$
$$\mu_4 = 1 - \delta\omega, \tag{A5}$$

with $\alpha = \sqrt{1 + \Gamma^2 + 2\Gamma\sigma\omega}$.

APPENDIX B: ADDITIONAL INFORMATION OF STOCHASTIC RESETTING DYNAMICS

Derivation of the modified dynamics under stochastic resetting. Here we provide some details for the derivation of the Eqs. (17) and (23) in the main text. Plugging the expansion formula

$$\boldsymbol{p}_{\rm in}^D(t_N) = p_{\rm in}^{D,ps} + \sum_{i\geqslant 2} a_i\lambda_i^N\boldsymbol{R}_i$$

and

$$\boldsymbol{\Delta}_{n\tau} = \boldsymbol{p}_{\rm in}^{D,ps} + \sum_{i\geqslant 2} d_i\lambda_i^n\boldsymbol{R}_i$$

into the renewal Eq. (10) for the demon's initial distribution,

$$\boldsymbol{p}_{\rm in}^D(r, t_N) = e^{-rN\tau}\boldsymbol{p}_{\rm in}^D(t_N) + (1 - e^{-r\tau})\sum_{n=0}^{N-1}[e^{-rn\tau}\boldsymbol{\Delta}_{n\tau}],$$

we reach that

$$\boldsymbol{p}^D(r, t_N) = e^{-rN\tau}\left[\boldsymbol{p}_{\rm in}^{D,ps} + \sum_{i\geqslant 2} a_i\lambda_i^n\boldsymbol{R}_i\right] + (1 - e^{-r\tau})\sum_{n=0}^{N-1} e^{-rn\tau}\left[\boldsymbol{p}_{\rm in}^{D,ps} + \sum_{i\geqslant 2} d_i\lambda_i^n\boldsymbol{R}_i\right] \tag{B1}$$

$$= \left[\boldsymbol{p}_{\rm in}^{D,ps} + \sum_{i\geqslant 2}\frac{1 - e^{-r\tau}}{1 - \lambda_i e^{-r\tau}} d_i\boldsymbol{R}_i\right] + \sum_{i\geqslant 2}\left[a_i - \frac{1 - e^{-r\tau}}{1 - \lambda_i e^{-r\tau}} d_i\right] e^{-rN\tau}\lambda_i^N\boldsymbol{R}_i \tag{B2}$$

$$= \boldsymbol{p}_{\rm in}^{D,ps} + \sum_{i\geqslant 2}\left\{\left[a_i - \frac{d_i(1 - e^{-r\tau})}{1 - \lambda_i e^{-r\tau}}\right] e^{-rN\tau} + \frac{d_i(1 - e^{-r\tau})}{1 - \lambda_i e^{-r\tau}}\cdot\lambda_i^{-N}\right\}\lambda_i^N\boldsymbol{R}_i \tag{B3}$$

$$\equiv \boldsymbol{p}_{\rm in}^{D,ps} + \sum_{i\geqslant 2} a_i(r, N)\lambda_i^N\boldsymbol{R}_i. \tag{B4}$$

Here, the modified coefficients $a_i(r, N)$ is obtained as

$$a_i(r, N) = \left[a_i - \frac{d_i(1 - e^{-r\tau})}{1 - \lambda_i e^{-r\tau}}\right] e^{-rN\tau} + \frac{d_i(1 - e^{-r\tau})}{1 - \lambda_i e^{-r\tau}}\cdot\lambda_i^{-N},$$

and the Eq. (B2) gives rise to the initial distribution of demon's new periodic steady state as

$$\boldsymbol{p}_{\rm in}^{D,ps}(r) = \lim_{N\to\infty}\boldsymbol{p}^D(r, t_N) = \boldsymbol{p}_{\rm in}^{D,ps} + \sum_{i\geqslant 2}\frac{1 - e^{-r\tau}}{1 - \lambda_i e^{-r\tau}} d_i\boldsymbol{R}_i, \tag{B5}$$

which is the Eq. (23) in the main text.

A protocol for the realization of the discrete-time stochastic resetting. This discrete-time resetting process may be realized as follows: The experimentalist can make resetting events occur in accordance with a continuous-time Poisson process characterized by the rate r_0. These events exclusively take place very close to the ending point of each interval, causing the demon to transition to the designated resetting state $\vec{\Delta}$. Letting δt represent the time window during which resetting events are likely to occur in the vicinity of interval endings, the likelihood of at least one such event transpiring can be expressed as $\gamma = 1 - e^{-r_0\delta t}$. We assume that $\delta t \ll \tau$ and $\delta t \propto \tau$, and define a (modified) resetting rate $r := r_0\delta t/\tau$. The impact of resetting events occurring near the end of an interval can be approximated by that of a single stochastic resetting

event taking place precisely at the end of the interval, with a probability of $\gamma = 1 - e^{-r\tau}$. That is, this event occurs with a probability of γ, while there is a probability of $1 - \gamma$ that it does not occur.

APPENDIX C: SPECTRAL ANALYSIS OF THE MATRIX $\mathcal{T}$

In this Appendix, we give some descriptions of the eigenvector expansion method used in the main text, i.e., doing spectral analysis of the evolution matrix $\mathcal{T}$ for the demon. $\mathcal{T}$ has right eigenvectors $\boldsymbol{R}_i$,

$$\mathcal{T}\boldsymbol{R}_i = \lambda_i \boldsymbol{R}_i \tag{C1}$$

and left eigenvectors $\boldsymbol{L}_i$ as

$$\boldsymbol{L}_i^{\mathrm{T}}\mathcal{T} = \lambda_i \boldsymbol{L}_i^{\mathrm{T}} \tag{C2}$$

with λ_i the eigenvalues, which are sorted as $1 = \lambda_1 > |\lambda_2| \geqslant |\lambda_3| \geqslant \ldots$ (we assume that λ_1 is not degenerate). The right eigenvector $\boldsymbol{R}_1$ with $1 = \lambda_1$ corresponds to the periodic steady state, so we write $\boldsymbol{R}_1 = \boldsymbol{p}_{\mathrm{in}}^{D,ps}$. According to the completeness relation, the initial state $\boldsymbol{p}_{\mathrm{in}}^{D}$ can be expanded as

$$\boldsymbol{p}_{\mathrm{in},0}^{D} = \boldsymbol{p}_{\mathrm{in}}^{D,ps} + \sum_{i>1} a_i \boldsymbol{R}_i, \tag{C3}$$

where

$$a_i = \frac{\boldsymbol{L}_i^{\mathrm{T}} \cdot \boldsymbol{p}_{\mathrm{in},0}^{D}}{\boldsymbol{L}_i^{\mathrm{T}} \cdot \boldsymbol{R}_i}. \tag{C4}$$

*Calculation of the i*th *coefficient* a_i. For an arbitrary matrix T, it can be demonstrated that any pair of left eigenvector and right eigenvector corresponding to different eigenvalues of the matrix are mutually orthogonal. Here is the proof (no degeneracy),

$$T\boldsymbol{R}_i = \lambda_i \boldsymbol{R}_i \Rightarrow \begin{cases} \boldsymbol{L}_j^{\mathrm{T}} T \boldsymbol{R}_i &= \lambda_i \boldsymbol{L}_j^{\mathrm{T}} \boldsymbol{R}_i \\ \boldsymbol{L}_j^{\mathrm{T}} T \boldsymbol{R}_i &= \lambda_j \boldsymbol{L}_j^{\mathrm{T}} \boldsymbol{R}_i \end{cases}$$
$$\Rightarrow (\lambda_i - \lambda_j)\boldsymbol{L}_j^{\mathrm{T}} \boldsymbol{R}_i = 0$$
$$\Rightarrow \boldsymbol{L}_j^{\mathrm{T}} \boldsymbol{R}_i = \left(\boldsymbol{L}_i^{\mathrm{T}} \cdot \boldsymbol{R}_i\right)\delta_{ij}.$$

Therefore, for an evolution starting at a given initial distribution $\boldsymbol{p}_{\mathrm{in}}^{D}$, we have that d_i is the corresponding overlap coefficient between the initial probability and the ith left eigenvector $\boldsymbol{L}_i^{\mathrm{T}}$. During the relaxation process, the initial distribution of the demon of the nth time interval, $\mathcal{T}^n \boldsymbol{p}_{\mathrm{in},0}^{D}$, can be written as

$$\mathcal{T}^n \boldsymbol{p}_{\mathrm{in},0}^{D} = \boldsymbol{p}_{\mathrm{in}}^{D,ps} + \sum_{i>1} d_i \lambda_i^n \boldsymbol{R}_i. \tag{C5}$$

Then,

$$\left\| \mathcal{T}^n \boldsymbol{p}_{\mathrm{in},0}^{D} - \boldsymbol{p}_{\mathrm{in}}^{D,ps} \right\|_1 = \sum_{i>1} d_i \|\lambda_i\|_1^n \|R_i\|_1, \tag{C6}$$

where $||\boldsymbol{p}|| \equiv \sum_i |p_i|$ is the L_1 norm. Thus, the relaxation timescale is typically characterized by

$$\tau_{\mathrm{rel}} = -\frac{1}{\ln|\lambda_2|}. \tag{C7}$$

Then it can be observed that a stronger effect (even shorter relaxation time) can occur: a process where there exists a specific initial distribution $\boldsymbol{\pi}_{\mathrm{in},0}^{D}$, such that

$$a_2|_{\boldsymbol{p}_{\mathrm{in},0}^{D} = \boldsymbol{\pi}_{\mathrm{in},0}^{D}} = \frac{\boldsymbol{L}_2^{\mathrm{T}} \cdot \boldsymbol{\pi}_{\mathrm{in},0}^{D}}{\boldsymbol{L}_2^{\mathrm{T}} \cdot \boldsymbol{R}_2} = 0.$$

APPENDIX D: EIGENVALUES OF THE INFORMATION REFRIGERATOR MODEL

Here we provide the expressions for the eigenvalues of the transition matrices for the two-state demon model. For the two-state demon with $\Gamma = 1$, the eigenvalues for $\mathcal{T}_{2\times 2}$ reads

$$\lambda_1 = 1, \tag{D1}$$

$$\lambda_2 = \frac{(\epsilon-2)\left(\frac{4\omega s e^{-2\tau}(\epsilon-1+\delta(\epsilon-2))}{\epsilon-2} + s(\delta\omega-1)(e^{(s-2)\tau}(s-2) - e^{(-s-2)\tau}(s+2))\right)}{4s(\epsilon-\omega+2\epsilon\omega-2)}, \tag{D2}$$

$$s \equiv \sqrt{2 + \frac{1-2\epsilon}{2-\epsilon}}. \tag{D3}$$

One can readily check that $\frac{\epsilon-2}{4s(\epsilon-\omega+2\epsilon\omega-2)} \geqslant 0$ and $s(\delta\omega-1)(e^{(s-2)\tau}(s-2) - e^{(-s-2)\tau}(s+2)) \geqslant 0$, since $\epsilon \in [0,\omega]$, $\omega \in [0,1]$ and $\delta \in [-1,1]$. When $\delta \geqslant 0$, $\epsilon - 1 + \delta(\epsilon-2) \leqslant \epsilon - 1 \leqslant 0$, so $\frac{4\omega s e^{-2\tau}(\epsilon-1+\delta(\epsilon-2))}{\epsilon-2} \geqslant 0$. Therefore, when $\delta \geqslant 0$, one always has $\lambda_2 \geqslant 0$ whatever the value of ω is.

APPENDIX E: ANOTHER EXAMPLE: THE THREE-STATE INFORMATION ENGINE

Here we provide another application of our framework. We use our strategy to optimize a three-state demon system (Fig. 7), i.e., the information engine proposed in [8]. In what follows we gives the model details. It can be defined that

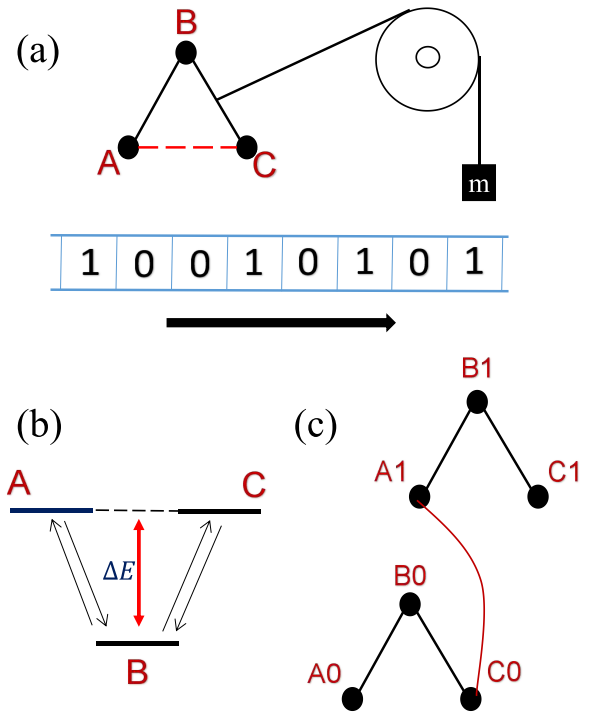

FIG. 7. The MIHE model. (a) The three-state demon interacts with a sequence of bits, a mass and a reservoir. (b) Schematic depiction of the demon, the bit and their composite six-state system. The state of the demon is indicated by an arrow pointing in one of the directions. The states B and A/C are characterized by an energy difference $\Delta E = E_u - E_d$ with $E_B = E_u$ and $E_A = E_C = E_d$. (c) Network depiction of the composite system, showing allowed transitions. The edge that connects A_1 and C_0 represents the coupling between the demon and bit.

the transition in the $A \to B \to C \to A$ direction is clockwise (CW), and the transition in the opposite direction is counterclockwise (CCW). The frequency difference between the CW transition and the CCW transition will cause the demon to display directional rotation. The demon and bit together form a composite system with six states, $A_0, \ldots, C_1$. When uncoupled to the bit, the demon can jump between states A and B, and B and C. Importantly, when the demon interacts with the bit, the demon is allowed to transition from C to A if the bit flips from 0 to 1 simultaneously, and vice versa, as shown in Fig. 7(c).

A positive positive external load $f = mg\Delta h/k_bT > 0$ (T is the temperature of the thermal reservoir and k_b is Boltzmann constant) is considered. It is assumed that the mass m is lifted by Δh every time the demon makes a transition $C \to A$, and lowered with $A \to C$. The transition rates with detailed balance can be written as

$$\frac{R_{A,B}}{R_{B,A}} = \frac{R_{C,B}}{R_{B,C}} = e^{-\Delta E/k_bT}, \tag{E1}$$

and

$$\frac{R_{A_1,C_0}}{R_{C_0,A_1}} = e^{-f}. \tag{E2}$$

For convenience, we set the $\Delta E \ll T \sim mg\Delta h$ so that $R_{ij} = 1$ for all transition rates except R_{A_1,C_0} and R_{C_0,A_1}. In particular, when the demon interacts with a fixed bit for a long enough time, both will reach equilibrium distribution simultaneously, which read

$$p^{eq}_{i,\, i\in\{A_0,B_0,C_0\}} = \tfrac{e^f}{Z},\ p^{eq}_{i,\, i\in\{A_1,B_1,C_1\}} = \tfrac{1}{Z} \tag{E3}$$

with $Z = 3(1 + e^f)$. For simplicity, a weight parameter ϵ is defined to describe the difference between the equilibrium probabilities for the bit after summing over the states of the demon,

$$\epsilon \equiv p^{eq}_0 - p^{eq}_1 = \tanh\left(\frac{f}{2}\right). \tag{E4}$$

Accelerating functionalization of the three-state demon through the first resetting strategy. In what follows (Fig. 8), we show that the first resetting strategy can be used to shorten the warm-up phase of the three-state demon by numerical results.

Eigenvalues of the three-state demon. The eigenvalues for transition matrix $\mathcal{T}_{3\times3}$ is given by

$$\lambda_1 = 1,\ \lambda_2 = \frac{\sigma[\sigma(4 + \sigma^{\sqrt{3}} + \sigma^{-\sqrt{3}}) + \delta\epsilon(6 - 4\sigma - \sigma^{1-\sqrt{3}} - \sigma^{1+\sqrt{3}})]}{6},\ \lambda_3 = \sigma^3,$$

with $\sigma = e^{-\tau} \in [0, 1]$. It can be readily proved that $\lambda_2 \geqslant \lambda_3 = \sigma^3$, here is the proof,

λ_2 can be rewritten as

$$\lambda_2 = \delta\epsilon\sigma + (1 - \delta\epsilon)\cdot\frac{4\sigma^2 + \sigma^2(\sigma^{\sqrt{3}} + \sigma^{-\sqrt{3}})}{6}, \tag{E5}$$

because $\delta \in [-1, 1]$ and $\epsilon \in [-1, 1]$, then we can let $a \equiv \delta\epsilon \in [-1, 1]$. Equivalently one just need to prove

$$\frac{\lambda_2}{\lambda_3} = a\frac{1}{\sigma^2} + (1 - a)\frac{4\frac{1}{\sigma} + \frac{1}{\sigma}\left[\left(\frac{1}{\sigma}\right)^{\sqrt{3}} + \left(\frac{1}{\sigma}\right)^{-\sqrt{3}}\right]}{6} \geqslant 1 \tag{E6}$$

$$\Leftrightarrow f(x, a) \equiv ax^2 + (1 - a)\frac{4x + x(x^{\sqrt{3}} + x^{-\sqrt{3}})}{6} \geqslant 1, \tag{E7}$$

with $x \equiv 1/\sigma \in [1, \infty)$. Note that it can be rewritten as

$$\begin{aligned} f(x, a) &= \left[x^2 - \frac{4x + x(x^{\sqrt{3}} + x^{-\sqrt{3}})}{6}\right]a \\ &\quad + \frac{4x + x(x^{\sqrt{3}} + x^{-\sqrt{3}})}{6} \\ &\equiv g(x)a + c(x), \end{aligned} \tag{E8}$$

and

$$\begin{aligned} g'(x) &= 2x - \frac{2}{3} + \frac{\sqrt{3}+1}{6}x^{\sqrt{3}} + \frac{1-\sqrt{3}}{6}x^{-\sqrt{3}} \\ &\geqslant 2 - \frac{2}{3} + \frac{\sqrt{3}+1}{6} + \frac{1-\sqrt{3}}{6} > 0, \end{aligned}$$

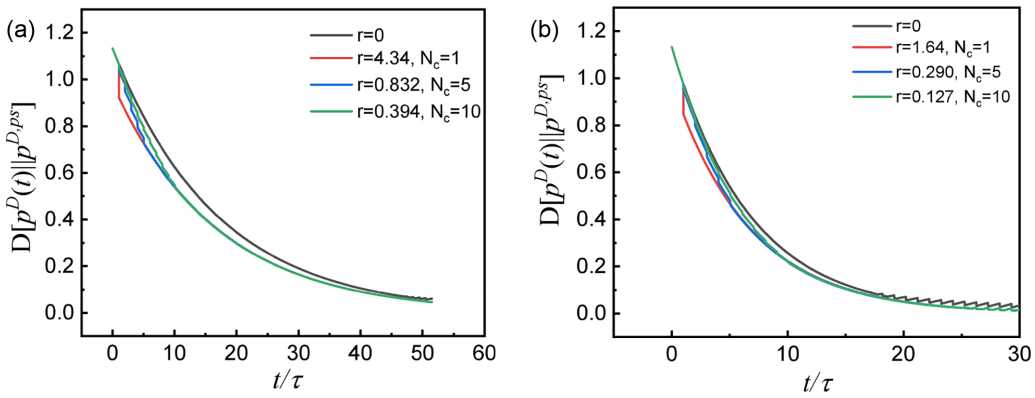

FIG. 8. The evolution of the three-state demon in warm-up phases. For each dynamics with different resetting rate r, the resetting is closed right after the critical time $t_c(r) = N_c(r)\tau$. The distance from the state $p^D(t)$ at time t to the periodic steady state $p^{D,ps}$ are plotted vs the cycle number t/τ. The dynamical parameters are given by (a) $\tau = 0.02,\ \delta = 1.0,\ \epsilon = 0.9$ and (b) $\tau = 0.05,\ \delta = 1.0,\ \epsilon = 0.9$.

thus, $g(x) \geqslant g(1) = 0$ and one can conclude that

$$f(x,a) \geqslant f(x,-1) = c(x) - g(x) = \frac{4x + x(x^{\sqrt{3}} + x^{-\sqrt{3}})}{3} - x^2 \equiv h(x). \tag{E9}$$

Because

$$h''(x) = \frac{3+\sqrt{3}}{3}x^{\sqrt{3}-1} + \frac{3-\sqrt{3}}{3}x^{-\sqrt{3}-1} - 2 \geqslant h''(1) = 0,$$

$$\Rightarrow h'(x) = \frac{4}{3} + \frac{\sqrt{3}+1}{3}x^{\sqrt{3}} + \frac{1-\sqrt{3}}{3}x^{-\sqrt{3}} - 2x \geqslant h'(1) = 0$$

$$\Rightarrow h(x) \geqslant h(1) = \frac{4+2}{3} - 1 = 1. \tag{E10}$$

Therefore, we have proved that $f(x,a) \geqslant f(x,-1) = h(x) \geqslant 1$, Q. E. D.

APPENDIX F: DERIVATION OF THE GENERALIZED SECOND LAW OF THERMODYNAMICS

During any interaction interval, the joint distribution of the interacting bit and the demon evolves according to the master equation

$$\frac{d\boldsymbol{p}}{dt} = \mathcal{R}\boldsymbol{p}.$$

Imagine that the interaction time τ is long enough ($\tau \to \infty$), then the combined system will finally reach a steady state (the entries of transition matrix $\mathcal{R}$ satisfy detailed balance condition, so it's an equilibrium state)

$$\boldsymbol{p}^{ss} = \frac{(1, \mu, \mu\nu, \mu^2\nu)^T}{1 + \mu + \mu\nu + \mu^2\nu}, \mu = \frac{1+\sigma}{1-\sigma}, \nu = \frac{1-\omega}{1+\omega}, \tag{F1}$$

which makes $\mathcal{R}\boldsymbol{p}^{ss} = \boldsymbol{0}$. When $\tau \to \infty$, the steady-state joint distribution $\boldsymbol{p}_{ss}$ is factorized as the product of marginal distributions $\boldsymbol{p}^{D,ss}$ and $\boldsymbol{p}^{B,ss}$, because the demon and bit are uncorrelated at the beginning of each interval by construction. And in this case distribution of bits can be regarded as an "effective initial distribution". That is,

$$p_{ij}^{ss} = p_i^{D,ss} p_j^{B,ss}, \quad i \in \{u, d\}, \quad j \in \{0, 1\}, \tag{F2}$$

where $\boldsymbol{p}^{\boldsymbol{D},\boldsymbol{ss}} = (1, \mu)^T/(1+\mu)$ and $\boldsymbol{p}^{\boldsymbol{B},\boldsymbol{ss}} = (1, \mu\nu)^T/(1+\mu\nu)$. When interaction time τ is finite, the combined system always relaxes towards this final steady state, though being interrupted by the advent of new bits and stochastic resetting events (one should note the similarity between resetting events for the demon and comings of new bits). Therefore, the distribution of combined system will get closer to the steady state $\boldsymbol{p}_{ss}$ at the end of an interval, compared to its distribution at the start of the same interval. That is, the relative entropy between any state $\boldsymbol{p}$ of the combined system and the steady state $\boldsymbol{p}_{ss}$,

$$D(\boldsymbol{p}||\boldsymbol{p}_{ss}) = \sum_k p_k \ln \frac{p_k}{p_k^{ss}} \geqslant 0, \tag{F3}$$

$$k \in \{0u, 0d, 1u, 1d\} \tag{F4}$$

as a distance function is a Lyapunov function, satisfying

$$\frac{d}{dt} D(\boldsymbol{p}||\boldsymbol{p}_{ss}) \leqslant 0. \tag{F5}$$

Let $\boldsymbol{p}_{\text{in}}$ and $\boldsymbol{p}_\tau$ denote the joint distribution at the start and at the end of a given interval respectively, and similarly define $\boldsymbol{p}_{\text{in}}^D, \boldsymbol{p}_\tau^D, \boldsymbol{p}_{\text{in}}^B$, and $\boldsymbol{p}_\tau^B$ for the marginal distributions of the demon and the bit. Then Eq. (F5) tells that

$$D(\boldsymbol{p}_{\text{in}}||\boldsymbol{p}_{ss}) - D(\boldsymbol{p}_\tau||\boldsymbol{p}_{ss}) \geqslant 0, \tag{F6}$$

whose physical interpretation is the initial joint state is farther from steady state than the final state at the end of the given interval is. Note that the left-hand side of the above equation is a standard expression of conventional entropy production during a period of time τ [59],

$$\Sigma_{[0,\tau]}^{\text{tot}} \equiv D(\boldsymbol{p}_{\text{in}}||\boldsymbol{p}_{ss}) - D(\boldsymbol{p}_\tau||\boldsymbol{p}_{ss}) \geqslant 0.$$

Using (F1) and (F3) one can rewrite the above equation as

$$S_\tau - S_0 + \sum_{i\in\{u,d\}} \left(p^D_{\tau,i} - p^D_{\text{in},i}\right) \ln p^{D,ss}_i + \sum_{i\in\{0,1\}} \left(p^B_{\tau,i} - p^B_{\text{in},i}\right) \ln p^{B,ss}_i \geqslant 0, \tag{F7}$$

where S_0 and S_τ refer to the information entropies of the joint distribution at the start and at the end of the current interval. What we need to consider is just the new periodic steady state in the presence of resetting. In this case, from the definition of the average production with resetting ϕ_r, $p^B_{\tau,1} - p^B_{\text{in},1} = -(p^B_{\tau,0} - p^B_{\text{in},0}) = \phi_r$, the last term of (F7) can be rewritten as

$$\sum_{i\in\{0,1\}} \left(p^B_{\tau,i} - p^B_{\text{in},i}\right) \ln p^{B,ss}_i = \phi_r \ln \mu\nu \tag{F8}$$

$$= Q_{c\to h}(\beta_h - \beta_c). \tag{F9}$$

The joint information entropy S can be decomposed as

$$S = S_D + S_B + I(D;B), \quad I(D;B) \geqslant 0, \tag{F10}$$

where S_D and S_B are marginal information entropy of the demon and the bit. Thus in our NPSS with resetting, Eq. (F7) gives [note that $I_0(D;B) = 0$ due to the uncorrelated initial distribution]

$$Q_{c\to h}(\beta_h - \beta_c) + \Delta S_B + \Delta S^{\text{rst}} \geqslant I_\tau(D;B) \geqslant 0, \tag{F11}$$

where

$$\Delta S_B = S_{B,\tau} - S_{B,0} = S_B(\delta') - S_B(\delta) = S_B(\delta - 2\phi_{\text{tot}}) - S_B(\delta), \tag{F12}$$

$$S_B(\delta) = -\sum_{i=0}^{1} p_i \ln p_i = -\frac{1-\delta}{2}\ln\frac{1-\delta}{2} - \frac{1+\delta}{2}\ln\frac{1+\delta}{2}, \tag{F13}$$

$$(\delta = p_0 - p_1,\ \delta' = p'_0 - p'_1) \tag{F14}$$

and

$$\Delta S^{\text{rst}} \equiv \Delta S_D + \sum_{i\in\{u,d\}} \left(p^{D,ps}_{\tau,i} - p^{D,ps}_{\text{in},i}\right) \ln p^{D,ss}_i, \tag{F15}$$

$$\Delta S_D = -\sum_{i=d}^{u} p^{D,ps}_{\tau,i} \ln p^{D,ps}_{\tau,i} + \sum_{i=d}^{u} p^{D,ps}_{\text{in},i} \ln p^{D,ps}_{\text{in},i} \tag{F16}$$

is the "resetting work" during a whole interval $[n\tau, (n+1)\tau]$ due to stochastic resetting. In the original periodic steady state without resetting, one has $\boldsymbol{p}^{D,ps}_\tau = \mathcal{T}\boldsymbol{p}^{D,ps}_{\text{in}} = \boldsymbol{p}^{D,ps}_{\text{in}}$ from definition of this state, so that the dissipated work (F16) vanishes. However, in the NPSS $\boldsymbol{p}^{D,ps}_\tau(r) = \mathcal{T}\boldsymbol{p}^{D,ps}_{\text{in}}(r) \neq \boldsymbol{p}^{D,ps}_{\text{in}}(r)$ according to the definition (23). In the NPSS, one can obtain

$$\boldsymbol{p}^{D,ps}_\tau(r) - \boldsymbol{p}^{D,ps}_{\text{in}}(r) = \mathcal{T}\boldsymbol{p}^{D,ps}_{\text{in}}(r) - \boldsymbol{p}^{D,ps}_{\text{in}}(r) \tag{F17}$$

$$= \frac{1-e^{-r\tau}}{1-\lambda_2 e^{-r\tau}} d_2(\mathcal{T}\boldsymbol{R}_2 - \boldsymbol{R}_2). \tag{F18}$$

Because $p^{D,ps}_{\tau,u} - p^{D,ps}_{\text{in},u} = -(p^{D,ps}_{\tau,d} - p^{D,ps}_{\text{in},d}) \equiv \Delta p^{D,ps}$, the second contribution of resetting work can be written as

$$\sum_{i=d}^{u} \left(p^{D,ps}_{\tau,i} - p^{D,ps}_{0,i}\right) \ln p^{D,ss}_i = \Delta p^{D,ps} \ln\mu = \beta_h \Delta p^{D,ps} \Delta E, \tag{F19}$$

thus the resetting work during each interval in the NPSS is given by

$$\Delta S^{\text{rst}} = \Delta S_D + \beta_h \Delta p^{D,ps} \Delta E. \tag{F20}$$

The above modified second law can also be derived from an integral fluctuation theorem for the stochastic entropy production. Following Seifert's spirit, the total stochastic entropy production in an interaction interval for a single trajectory $\Gamma_{i\to j}$ starting in state i at initial time and ending in state j at time τ is defined as ($i, j \in \{0u, 0d, 1u, 1d\}$)

$$\sigma(\Gamma_{i\to j}) = \ln\frac{p_i(0)p(\Gamma_{i\to j})}{p_j(\tau)p(\Gamma^\dagger_{j\to i})}, \tag{F21}$$

$$= \ln\left[\frac{p_i(0)}{p_j(\tau)} \prod_{k,l\in\Gamma_{i\to j}} \left(\frac{R_{kl}}{R_{lk}}\right)^{n_{kl}}\right], \tag{F22}$$

which naturally gives rise to an integral fluctuation theorem

$$\langle e^{-\sigma(\Gamma_{i\to j})}\rangle = \sum_{i,j}\int d\Gamma_{i\to j} p_i(0) p(\Gamma_{i\to j}) e^{-\sigma(\Gamma_{i\to j})} = \sum_{i,j}\int d\Gamma_{i\to j} p_j(\tau) p(\Gamma^\dagger_{j\to i}) = \sum_{i,j}\int d\Gamma^\dagger_{j\to i} p_j(\tau) p(\Gamma^\dagger_{j\to i}) = 1. \tag{F23}$$

Then using Jensen equality, it follows that

$$\Sigma^{\text{tot}}_{[0,\tau]} \equiv \langle\sigma(\Gamma_{i\to j})\rangle \geqslant 0.$$

It has been proven that [60]

$$\left\langle \frac{d}{dt}\sigma(\Gamma_{i\to j})\right\rangle = [R_{ij}p_j(t) - R_{ji}p_i(t)] \ln\frac{R_{ij}p_j(t)}{R_{ji}p_i(t)}. \tag{F24}$$

Then we have

$$\langle\sigma(\Gamma_{i\to j})\rangle = \int_0^\tau \sum_{i>j} [R_{ij}p_j(t) - R_{ji}p_i(t)] \ln\frac{R_{ij}p_j(t)}{R_{ji}p_i(t)} = -\int_0^\tau \frac{d}{dt} D(\boldsymbol{p}(t)||\boldsymbol{p}_{ss}) = Q_{c\to h}(\beta_h - \beta_c) + \Delta S_B + \Delta S^{\text{rst}} - I_\tau(D;B) \geqslant 0,$$

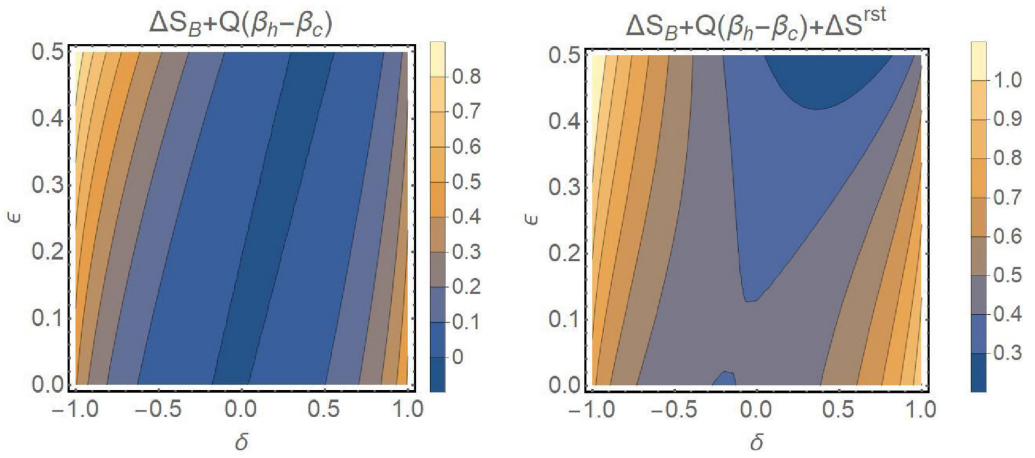

FIG. 9. Contour plots of the values of (a) $Q_{c\to h}(\beta_h-\beta_c)+\Delta S_B$ and (b) $Q_{c\to h}(\beta_h-\beta_c)+\Delta S_B+\Delta S^{\rm rst}$.

where in the second line the detailed balance condition $R_{ij}p_j^{ss}=R_{ji}p_i^{ss}$ has been used [61]. Finally, we show the contour plots for $Q_{c\to h}(\beta_h-\beta_c)+\Delta S_B$ and $Q_{c\to h}(\beta_h-\beta_c)+\Delta S_B+\Delta S^{\rm rst}$ as demonstration of the generalized second law (Fig. 9).

[1] J. C. Maxwell and P. Pesic, *Theory of Heat* (Courier Corporation, New York, 1871).

[2] R. Landauer, Irreversibility and heat generation in the computing process, IBM J. Res. Dev. **5**, 183 (1961).

[3] C. H. Bennett, The thermodynamics of computation—A review, Int. J. Theor. Phys. **21**, 905 (1982).

[4] A. Rex, Maxwell's demon—A historical review, Entropy **19**, 240 (2017).

[5] J. Parrondo, J. M. Horowitz, and T. Sagawa, Thermodynamics of information, Nat. Phys. **11**, 131 (2015).

[6] L. Szilard, Über die entropieverminderung in einem thermodynamischen system bei eingriffen intelligenter wesen, Z. Angew. Phys. **53**, 840 (1929).

[7] R. P. Feynman, R. B. Leighton, and M. Sands, *The Feynman Lectures on Physics, Vol. I: The New Millennium Edition: Mainly Mechanics, Radiation, and Heat* (Basic Books, New York, 2011).

[8] D. Mandal and C. Jarzynski, Work and information processing in a solvable model of Maxwell's demon, Proc. Natl. Acad. Sci. USA **109**, 11641 (2012).

[9] T. Sagawa and M. Ueda, Nonequilibrium thermodynamics of feedback control, Phys. Rev. E **85**, 021104 (2012).

[10] D. Mandal, H. Quan, and C. Jarzynski, Maxwell's refrigerator: An exactly solvable model, Phys. Rev. Lett. **111**, 030602 (2013).

[11] P. Strasberg, G. Schaller, T. Brandes, and C. Jarzynski, Second laws for an information driven current through a spin valve, Phys. Rev. E **90**, 062107 (2014).

[12] J. V. Koski, A. Kutvonen, I. M. Khaymovich, T. Ala-Nissila, and J. P. Pekola, On-chip Maxwell's demon as an information-powered refrigerator, Phys. Rev. Lett. **115**, 260602 (2015).

[13] A. M. Jurgens and J. P. Crutchfield, Functional thermodynamics of Maxwellian ratchets: Constructing and deconstructing patterns, randomizing and derandomizing behaviors, Phys. Rev. Res. **2**, 033334 (2020).

[14] T. Joseph and Kiran V, Efficiency estimation for an equilibrium version of the Maxwell refrigerator, Phys. Rev. E **103**, 022131 (2021).

[15] D. Bhattacharyya and C. Jarzynski, From a feedback-controlled demon to an information ratchet in a double quantum dot, Phys. Rev. E **106**, 064101 (2022).

[16] L. He, A. Pradana, J. W. Cheong, and L. Y. Chew, Information processing second law for an information ratchet with finite tape, Phys. Rev. E **105**, 054131 (2022).

[17] H. Sandberg, J.-C. Delvenne, N. J. Newton, and S. K. Mitter, Maximum work extraction and implementation costs for nonequilibrium Maxwell's demons, Phys. Rev. E **90**, 042119 (2014).

[18] G. Manzano, D. Subero, O. Maillet, R. Fazio, J. P. Pekola, and É. Roldán, Thermodynamics of gambling demons, Phys. Rev. Lett. **126**, 080603 (2021).

[19] N. Freitas M. Esposito, Maxwell demon that can work at macroscopic scales, Phys. Rev. Lett. **129**, 120602 (2022).

[20] S. Ryu, R. López, and R. Toral, Quantum consensus dynamics by entangling Maxwell demon, New J. Phys. **24**, 033028 (2022).

[21] S. Deffner, Information-driven current in a quantum Maxwell demon, Phys. Rev. E **88**, 062128 (2013).

[22] K. Poulsen, M. Majland, S. Lloyd, M. Kjaergaard, and N. T. Zinner, Quantum Maxwell's demon assisted by non-Markovian effects, Phys. Rev. E **105**, 044141 (2022).

[23] M. R. Evans and S. N. Majumdar, Diffusion with stochastic resetting, Phys. Rev. Lett. **106**, 160601 (2011).

[24] S. Gupta, S. N. Majumdar, and G. Schehr, Fluctuating interfaces subject to stochastic resetting, Phys. Rev. Lett. **112**, 220601 (2014).

[25] S. Reuveni, Optimal stochastic restart renders fluctuations in first passage times universal, Phys. Rev. Lett. **116**, 170601 (2016).

[26] A. Pal and S. Reuveni, First passage under restart, Phys. Rev. Lett. **118**, 030603 (2017).

[27] S. Belan, Restart could optimize the probability of success in a Bernoulli trial, Phys. Rev. Lett. **120**, 080601 (2018).

[28] A. Chechkin and I. M. Sokolov, Random search with resetting: A unified renewal approach, Phys. Rev. Lett. **121**, 050601 (2018).

[29] A. Pal, I. Eliazar, and S. Reuveni, First passage under restart with branching, Phys. Rev. Lett. **122**, 020602 (2019).

[30] A. Miron and S. Reuveni, Diffusion with local resetting and exclusion, Phys. Rev. Res. **3**, L012023 (2021).

[31] B. De Bruyne, S. N. Majumdar, and G. Schehr, Optimal resetting Brownian bridges via enhanced fluctuations, Phys. Rev. Lett. **128**, 200603 (2022).

[32] B. De Bruyne, J. R. Furling, and S. Redner, Optimization in first-passage resetting, Phys. Rev. Lett. **125**, 050602 (2020).

[33] É. Roldán, A. Lisica, D. Sánchez-Taltavull, and S. W. Grill, Stochastic resetting in backtrack recovery by RNA polymerases, Phys. Rev. E **93**, 062411 (2016).

[34] D. M. Busiello, D. Gupta, and A. Maritan, Inducing and optimizing Markovian Mpemba effect with stochastic reset, New J. Phys. **23**, 103012 (2021).

[35] D. Gupta, C. A. Plata, and A. Pal, Work fluctuations and Jarzynski equality in stochastic resetting, Phys. Rev. Lett. **124**, 110608 (2020).

[36] D. M. Busiello, D. Gupta, and A. Maritan, Entropy production in systems with unidirectional transitions, Phys. Rev. Res. **2**, 023011 (2020).

[37] D. Gupta and D. M. Busiello, Tighter thermodynamic bound on the speed limit in systems with unidirectional transitions, Phys. Rev. E **102**, 062121 (2020).

[38] A. Pal, S. Reuveni, and S. Rahav, Thermodynamic uncertainty relation for systems with unidirectional transitions, Phys. Rev. Res. **3**, 013273 (2021).

[39] J. Fuchs, S. Goldt, and U. Seifert, Stochastic thermodynamics of resetting, Europhys. Lett. **113**, 60009 (2016).

[40] A. Pal and S. Rahav, Integral fluctuation theorems for stochastic resetting systems, Phys. Rev. E **96**, 062135 (2017).

[41] M. R. Evans, S. N. Majumdar, and G. Schehr, Stochastic resetting and applications, J. Phys. A: Math. Theor. **53**, 193001 (2020).

[42] S. Gupta and A. M. Jayannavar, Stochastic resetting: A (very) brief review, Front. Phys. **10**, 789097 (2022).

[43] Z. Cao, R. Bao, J. Zheng, and Z. Hou, Fast functionalization with high performance in the autonomous information engine, J. Phys. Chem. Lett. **14**, 66 (2023).

[44] J. Liu, K. A. Jung, and D. Segal, Periodically driven quantum thermal machines from warming up to limit cycle, Phys. Rev. Lett. **127**, 200602 (2021).

[45] A. Gal and O. Raz, Precooling strategy allows exponentially faster heating, Phys. Rev. Lett. **124**, 060602 (2020).

[46] I. Klich, O. Raz, O. Hirschberg, and M. Vucelja, Mpemba index and anomalous relaxation, Phys. Rev. X **9**, 021060 (2019).

[47] A. Kumar and J. Bechhoefer, Exponentially faster cooling in a colloidal system, Nature (London) **584**, 64 (2020).

[48] Z. Lu and O. Raz, Nonequilibrium thermodynamics of the Markovian Mpemba effect and its inverse, Proc. Natl. Acad. Sci. USA **114**, 5083 (2017).

[49] A. Santos and A. Prados, Mpemba effect in molecular gases under nonlinear drag, Phys. Fluids **32**, 072010 (2020).

[50] M. Baity-Jesi, E. Calore, A. Cruz, L. A. Fernandez, J. M. Gil-Narvión, A. Gordillo-Guerrero, D. Iñiguez, A. Lasanta, A. Maiorano, E. Marinari, *et al.*, The Mpemba effect in spin glasses is a persistent memory effect, Proc. Natl. Acad. Sci. USA **116**, 15350 (2019).

[51] C. D. Meyer, *Matrix Analysis and Applied Linear Algebra*, Vol. 71 (SIAM, Philadelphia, 2000).

[52] A. C. Barato and U. Seifert, Thermodynamic uncertainty relation for biomolecular processes, Phys. Rev. Lett. **114**, 158101 (2015).

[53] T. R. Gingrich, J. M. Horowitz, N. Perunov, and J. L. England, Dissipation bounds all steady-state current fluctuations, Phys. Rev. Lett. **116**, 120601 (2016).

[54] M. Polettini, A. Lazarescu, and M. Esposito, Tightening the uncertainty principle for stochastic currents, Phys. Rev. E **94**, 052104 (2016).

[55] K. Liu, Z. Gong, and M. Ueda, Thermodynamic uncertainty relation for arbitrary initial states, Phys. Rev. Lett. **125**, 140602 (2020).

[56] T. Koyuk and U. Seifert, Thermodynamic uncertainty relation for time-dependent driving, Phys. Rev. Lett. **125**, 260604 (2020).

[57] R. Yin and E. Barkai, Restart expedites quantum walk hitting times, Phys. Rev. Lett. **130**, 050802, (2023).

[58] G. Perfetto, F. Carollo, M. Magoni, and I. Lesanovsky, Designing nonequilibrium states of quantum matter through stochastic resetting, Phys. Rev. B **104**, L180302 (2021).

[59] N. Shiraishi and K. Saito, Information-theoretical bound of the irreversibility in thermal relaxation processes, Phys. Rev. Lett. **123**, 110603 (2019).

[60] U. Seifert, Stochastic thermodynamics, fluctuation theorems, and molecular machines, Rep. Prog. Phys. **75**, 126001 (2012).

[61] J. M. Horowitz and J. L. England, Information-theoretic bound on the entropy production to maintain a classical nonequilibrium distribution using ancillary control, Entropy **19**, 333 (2017).